REPORT DOCUMENTATION PAGE

Form Approved
OMB No. 0704-0188

1. REPORT DATE *(DD-MM-YYYY)*	**2. REPORT TYPE**	**3. DATES COVERED** *(From - To)*
22-08-2013	Final Technical Report	01-June-2010 to 31-May-2013

4. TITLE AND SUBTITLE

Separation of Armchair SWNTs by Using Polymer Conformation Guided Assembly

5a. CONTRACT NUMBER

5b. GRANT NUMBER
FA9550-10-1-0254

5c. PROGRAM ELEMENT NUMBER

6. AUTHOR(S)

Pang, Yi;
Wang, Xiao-Qian;
Sokolov, Alexei P.

5d. PROJECT NUMBER

5e. TASK NUMBER

5f. WORK UNIT NUMBER

7. PERFORMING ORGANIZATION NAME(S) AND ADDRESS(ES)

University of Akron,
Clark Atlanta University,
University of Tennessee

8. PERFORMING ORGANIZATION REPORT NUMBER

9. SPONSORING / MONITORING AGENCY NAME(S) AND ADDRESS(ES)

Office of Naval Research
Chicago Regional Office
230 South Dearborn, Room 380
Chicago, IL 60605

10. SPONSOR/MONITOR'S ACRONYM(S)

11. SPONSOR/MONITOR'S REPORT NUMBER(S)

12. DISTRIBUTION / AVAILABILITY STATEMENT

Distribution A

13. SUPPLEMENTARY NOTES

14. ABSTRACT

Isolation of single-walled carbon nanotubes (SWNTs) remains to be a key step for realization of the true potential of SWNTs, since the physical properties of SWNTs are dependent on the tube's chirality index (n, m). Polymers with enhanced helical conformation are found to be an efficient sorting mechanism for SWNTs, as the cavity of polymer's helical conformation can be tailored to facilitate an intimate interaction between polymer and SWNTs. Poly[(m-phenylenevinylene) (PmPV) demonstrates that the polymer helical conformation can be controlled to sort the SWNTs by their diameters. Poly [(m-phenyleneethynylene)-alt-(p-phenyleneethynylene)] (PPE) reveals the intriguing selectivity toward tube (6,5), illustrating the impact of carbon-carbon triple bonds on the SWNTs selectivity. In another approach, polyethyleneimine (PEI) is found to exhibit selective interaction with semiconducting SWNTs. By using this property, cellulose impregnated with PEI is found to be a column packing materials for separation of metallic SWNTs from a raw HiPco sample. Analysis by AFM, 2D fluorescence and UV-vis-NIR absorption spectra suggests that the metallic SWNTs (13,4) can be separated from the armchair SWNTs (10,10) and (9,9).

15. SUBJECT TERMS

carbon nanotube, polymer, separation

16. SECURITY CLASSIFICATION OF:			**17. LIMITATION OF ABSTRACT**	**18. NUMBER OF PAGES**	**19a. NAME OF RESPONSIBLE PERSON**
a. REPORT	**b. ABSTRACT**	**c. THIS PAGE**	SAR	42	Yi Pang
					19b. TELEPHONE NUMBER *(include area code)* (330)-972-8263

Standard Form 298 (Rev. 8-98)
Prescribed by ANSI Std. Z39.18

Final Performance Report

Project Title: Separation of Armchair SWNTs by Using Polymer Conformation-Guided Assembly.

Grant No.: FA9550-10-1-0254

PIs: Dr. Yi Pang, Department of Chemistry, University of Akron

Dr. Xiaoqian Wang, Department of Physics, Clark Atlanta University

Dr. Alexei P. Sokolov, University of Tennessee

Table of Content

Introduction

Single-walled carbon nanotubes (SWNTs) are among the most promising new materials in the focus of nanoscience and nanotechnology, as they exhibit superior mechanical[1] and electrical properties.[2,3] The chemical stability and robust physical properties of individual SWNT are uniquely dependent on the chiral indices (*n*,*m*) which determine the tube's diameters.[4] Unfortunately, tubes in the as-prepared sample are generally grown as a mixture of different SWNTs. In order to access SWNT of single (*n*,*m*) chirality, a post-synthesis process becomes necessary to separate different SWNTs. Individualization of a specific chiral SWNT from their mixture remains a major challenge, due to their structural similarity between SWNT species.[5]

Significant efforts have been developed to sort different (*n*,*m*) SWNTs, and the activity prior 2009 has been extensively reviewed.[5] Among the prominent approaches to isolate SWNTs include using flavin,[6] single-stranded DNA,[7] density-gradient ultracentrifugation,[8,9] dextran-based size-exclusion gel,[10] and polymers.[11,12,13] Despite significant progress in recent years, the current methodologies suffer from either high cost such as in DNA separation,[7] or low separation efficiency. While the dextran-based size-exclusion gel[10] can separate *semi*-SWNTs, it does not differentiate different *met*-SWNTs. Among the existing methods, the polymer-based isolation remains to be one of the most promising strategies, as size-exclusion chromatography is one of the most popular methods for separation of different kinds of macromolecules.[14]

Selective dispersion of SWNTs is dependent on the selective interaction of a dispersion reagent with a specific type of nanotube(s). Due to the curvature of the nanotube surface, an optimum interaction often involves a helical assembly of dispersion reagent on a SWNT. For example, selectivity dispersion of (8,6) SWNT by flavin mononucleotide[6] is dependent on the helical assembly of flavin. Helical wrapping of polyfluorene **1** on SWNTs is also thought to play an important role in the selective dispersion of SWNTs.[15] On the basis of these observations, it is reasonable to assume that a polymer with a helical conformation could provide an optimum interaction for a specific SWNT, as the polymer's conformation could bring the chain segments to a unique arrangement for an intimate contact with the SWNT surface. In addition, the polymer's conformational cavity could be controlled to match the diameter of an SWNT, thereby adding another parameter to facilitate the separation. The study is thus focusing on the impact of polymer conformation-guided assembly on the selective dispersion of SWNTs.

Some π-conjugated polymers have shown to exhibit good selectivity toward certain SWNTs, which are summarized in Table 1. Nicholas[15] and Kappe[16] have independently reported that fluorene-based polymer **1a** is selective to (7,5) and (9,7), while **2** is selective to (10,5).[16] Nakashima et al.[17] report that nanotube selectivity can be influenced by changing the copolymer composition ratio (x:y ratio in **3**). Inclusion of other segments in polyfluorene appears to play an important role in modifying the selectivity. For example, Nakashima et al.[13] have reported that the bipyridine-containing co-polymer **4** exhibits high selectivity to the small diameter (6,5)-SWNT, in contrast to **3** that selects a group of SWNTs with emission at ~1500 nm (by Tange et al.).[18] Other important example includes regioregular poly(3-methyl-4-decyl-thiophene-2,5-diyl) **6**, which can enrich *semi*-SWNTs that can be used in fabrication of transistors and solar cells.[19] While the helical wrapping of π-conjugated polymers has been used to describe the polymer-nanotube interaction,[15] little is explored in using the helical conformation to facilitate the SWNTs isolation.

Table 1. Separation of SWNTs by Selective Dispersion Using Polymeric Reagents

Separated SWNTs	Polymers used	comments	ref
(7,5), (7,6), (10,5), (9,7)	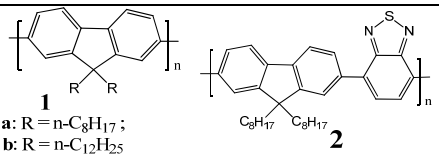 **1** **a**: R = n-C_8H_{17} ; **b**: R = n-$C_{12}H_{25}$ **2**	enrich SWNTs to about 60-90% in toluene solvent.	[15,16,]
(7,5), (7,6), (8,6), (8,7), (9,7), (10,3)	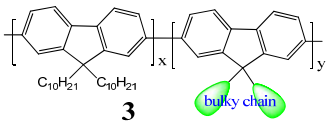 **3**	as the ratio x:y decreases, the selectivity to (7,5), (7,6) and (8,6) decreases, while the selectivity to (8,7), (9,7) and (10,3) increases.	[17]
(13,5), (10,8), (14,3)	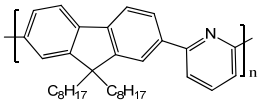 **4**	A group of SWNTs with emission at ~1500 nm are enriched in toluene solvent.	[18]
(6,5)	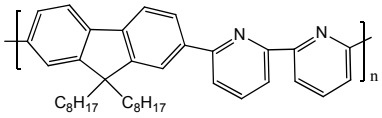 **5**	upto 96% enriched in *p*-xylene and *m*-xylene solvents.	[13]
semi-SWNTs	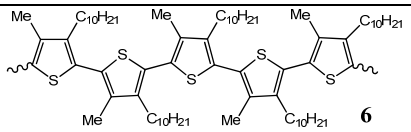 **6**	highly selective dispersion of semi-SWNTs enables direct film preparation of SWNTs/polythiophenes	[19]

1.0 Achieving Diameter-Selective Dispersion of SWNTs by Using Water-Soluble Poly(phenylene vinylene) to Control Helical Conformation Cavity

Sorting SWNTs by diameters is a useful strategy, as it can separate nanotubes into different groups. Since each group will contain fewer SWNTs, the diameter-based sorting will simplify the problem of separating SWNTs into individual tubes of single chirality. In order to use the polymer conformation to aid the diameter-sorting process, the polymer is required to exhibit the helical conformation that provides a suitable cavity to host the SWNTs of a comparable diameter.

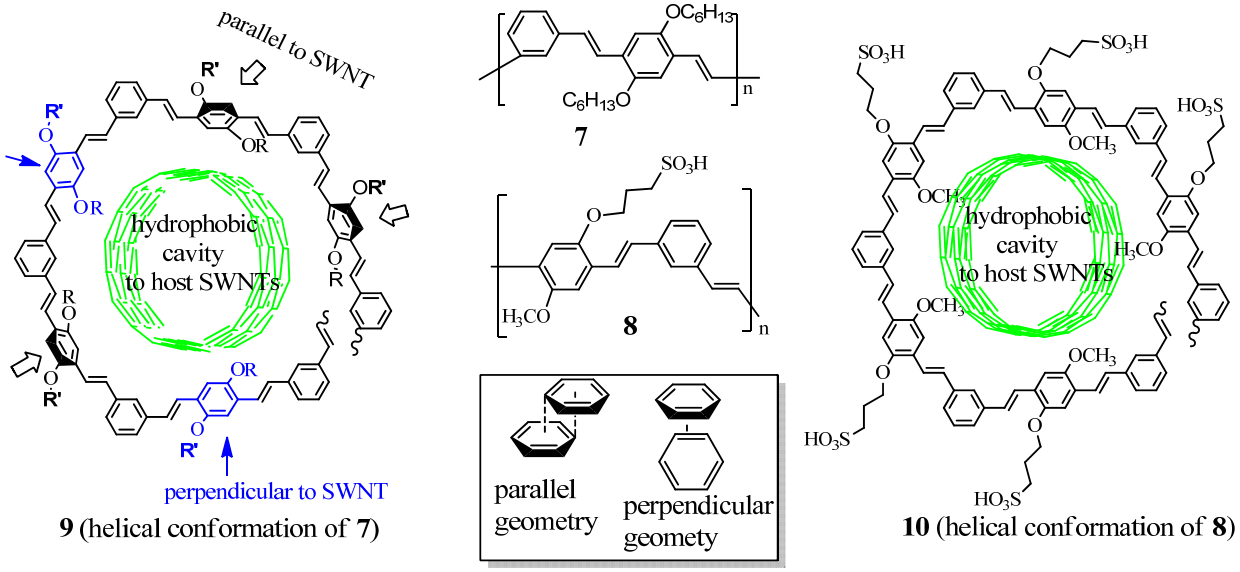

Figure 1. Structure of PmPVs **7** and **8**, and proposed respective helical conformations **9** and **10** when being wrapped on a (7,5) SWNT. The inset shows the parallel and perpendicular alignment of two benzene rings. The $-OCH_3$ groups in **10** are pointing inward to provide a defined cavity size.

Poly[(*m*-phenylenevinylene)-*alt*-(*p*-phenylenevinylene)] (P*m*PV) **7** represents an interesting π-conjugated polymer, whose backbone exhibits relative flexibility (Mark-Houwink constant $\alpha \approx 0.85\text{-}1.0$)[20] and tends to adopt a helical conformation when dispersing SWNTs.[21] The *para*-phenylene units of PmPV **7** can be aligned either parallel or perpendicular to SWNT surface (Figure 1) as a modeling study suggests. In this study, the polymer conformation is tailored to favor the perpendicular alignment of the π-conjugated segments to SWNT surface (see conformation **10**), thereby attenuating its π–π interaction with SWNTs. The strategy is based on

the synthesis of P*m*PV **8**, which bears the water-soluble groups to promote the helical conformation in aqueous solution. In sharp contrast to P*m*PV **7** which is known to be a good dispersing reagent but exhibits little selectivity toward metallic SWNTs,[21] P*m*PV **8** reveals drastically improved selectivity in sorting the SWNTs on the basis of tube's diameters.[22]

Results and Discussion

The water-soluble PmPV **8** was synthesized by using Wittig condensation of **11** with isophthaldehyde (Scheme 1). ^{1}H NMR of PmPV **8** (Figure 2) revealed that the polymer had a regular structure as proposed. The minor aromatic singlet at 7.75 ppm was attributed to H_e, while the remaining aromatic and vinyl signals occurred as a broad multiple peaks at about 7.45 ppm. The protons of $–CH_2O–$ (at 4.24 ppm) and $–OCH_3$ (at 3.94 ppm) each occurred as a broad single peak, indicating that the vinylene bonds were mainly in the *trans*-configuration.[20]

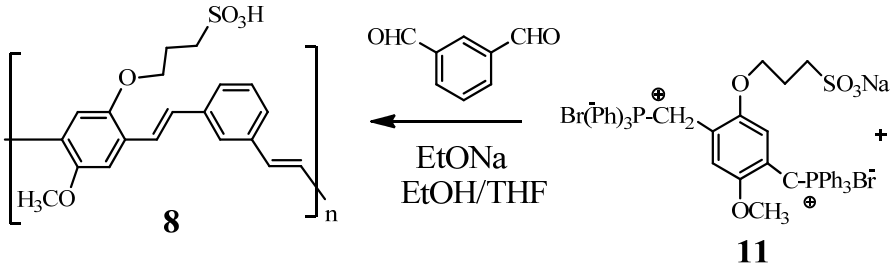

Scheme 1. Synthesis of water-soluble PmPV **8**.

Polymer wrapping. The SWNTs were then dispersed by using PmPV solution in deionized water. In a typical dispersion procedure,[21] 3 mg of SWNTs sample and 20 mL of PmPV in deionized water solution (concentration = 26.2 mg/mL) was mixed, and the mixture was sonicated at 0°C for one and half hour. The supernatant solution was then separated from the sediment by centrifugation at 7000 g.

^{1}H NMR of the supernatant solution revealed that the polymer in SWNT/PmPV had strong interaction with SWNTs. Upon forming complex with SWNTs, the methylene protons H_b, H_c and H_d of **8** were shifted upfield by about 1 ppm (Figure 2, bottom spectrum). The observed upfield shift from protons H_b–H_d was consistent with the chain assembly arising from polymer/SWNT interaction, as the free acetone signal at 2.07 ppm was not changed in the presence of SWNTs. The signal of $–OCH_3$, however, was not detected. The signals of vinyl

and phenyl protons were dramatically decreased, indicating the intimate chain interaction with SWNT surface. The aromatic protons that are closely associated with SWNTs are known to become undetectable,[23] due to the presence of paramagnetic particle in SWNT sample. Disappearance of $-OCH_3$ signals, but not H_b ($-OCH_2-$), suggested that the former had a closer interaction with the guest SWNT than the latter, in agreement with the proposed helical wrapping model as shown in **10** (Figure 1).

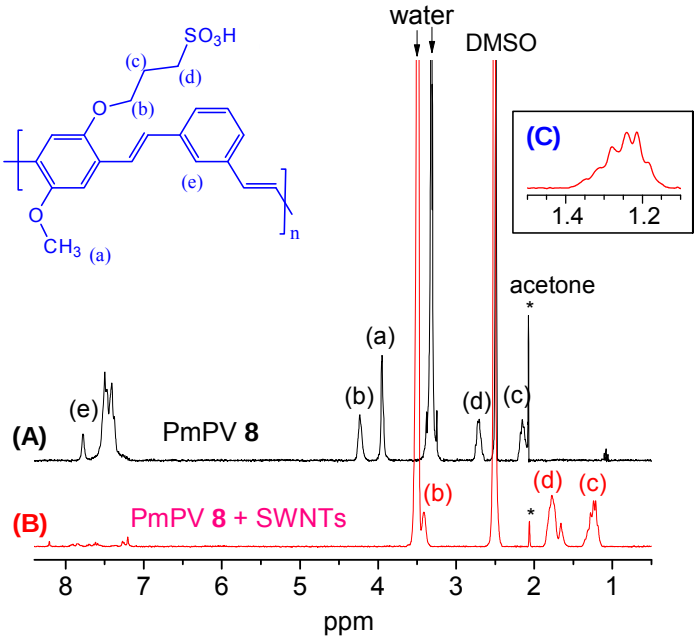

Figure 2. ^{1}H NMR spectra of PmPV **8** (A) and its complex with SWNTs (B) in deuterated DMSO solvent. The protons are labeled by letters a-f. In the bottom spectrum, one drop of D_2O was added to slightly shift the water signal away from the $-OCH_2-$ signal, where the solvent suppression at 3.49 ppm resulted in a lower proton intensity at 3.41 ppm. The starred signal at 2.07 ppm was due to trace acetone in the NMR tube. The inset is the expanded region for proton (c) of spectrum (B), displaying the coupling with adjacent protons.

Spectroscopic evidence for selective SWNT dispersion. Raman spectra of SWNTs/PmPV revealed that polymer **8** had quite high selectivity in dispersing (7,5) SWNTs (Figure 3a), in sharp contrast to PmPV **7**.[21] Raman spectra measured with green light (λ=514 nm) showed that the metallic (9,3) SWNT was also selected by the polymer (Figure 3b). Plotting the Raman intensity changes for each SWNT clearly revealed that the polymer selectively enriched the SWNT of smaller diameter (d<0.9 nm, Figure 4).

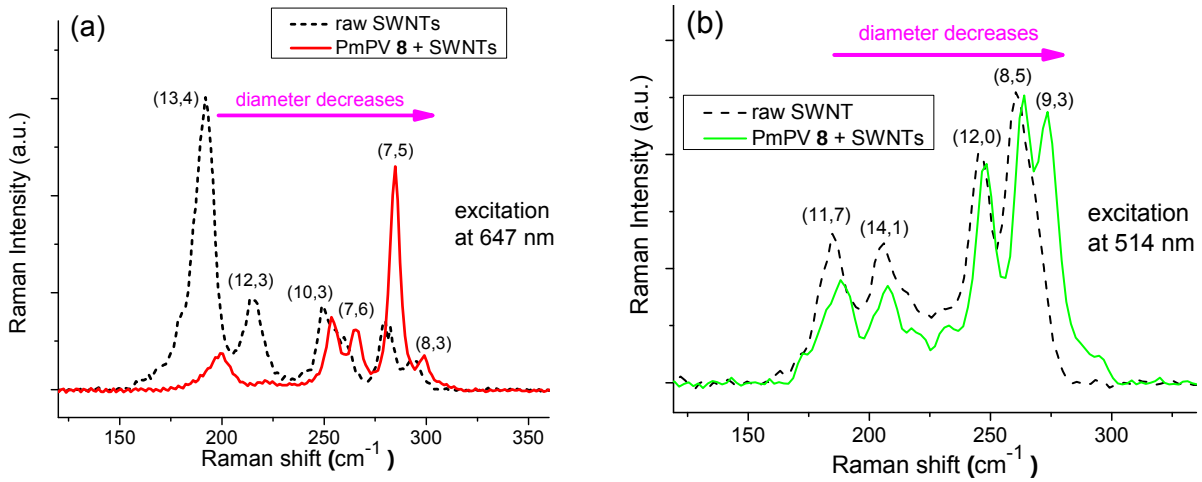

Figure 3 Raman spectra of raw SWNTs and SWNTs/PmPV **8** when the samples were excited with a laser at 647 nm (a) or a laser at 514 nm (b).

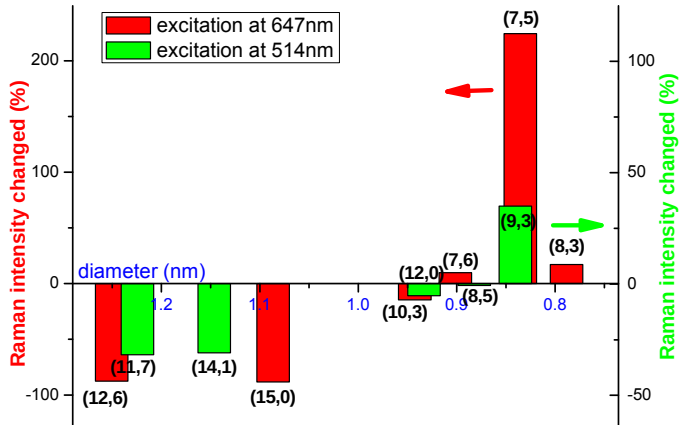

Figure 4. Relative SWNT population change by using PmPV **8** . The plot is constructed by using Raman intensity change for each SWNT shown in Figure 3.

The selectivity was further observed from 2D fluorescence spectra (Figure 5). The signals from SWNTs/PmPV sample were quite weak, as the nanotubes tended to precipitate from the supernatant aqueous solution of polymer/SWNTs. The small diameter (6,5) SWNT was clearly enriched in the SWNTs/PmPV dispersion. While the fluorescence intensity of (7,5) was weaker than that of (7,6) SWNT in the raw sample, the signal of (7,5) was increased to a comparable level in the SWNTs/PmPV complex, in agreement with what was seen in Raman. It appeared that the polymer **8** selectively extracted the SWNTs of smaller diameter, (6,5) and (7,5) SWNTs

(d=0.76 and 0.83 nm, respectively).[24,21] The spectra also revealed that those SWNTs with relative large diameters, such as (8,6) and (9,5) (d=0.97 and 0.98, respectively), were effectively removed.

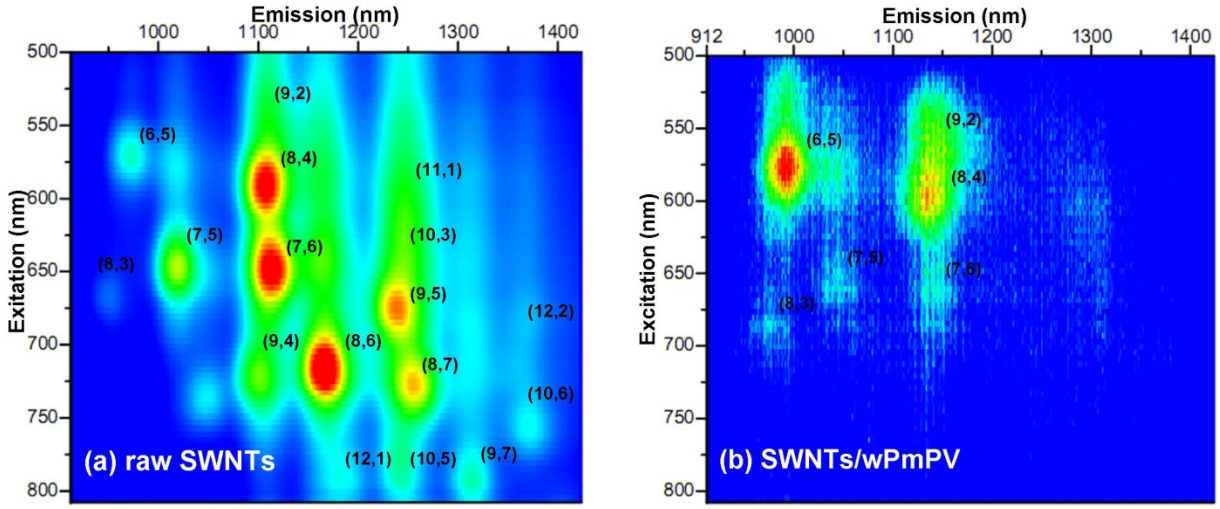

Figure 5. 2D photoluminescence (PL) of SWNT samples (excitation: 500-840 nm; emission: 912-1415 nm). (a) Raw SWNTs was dispersed with addition of sodium dodecylbenzene sulfonate (SDBS) (6% in water). (b) SWNTs were dispersed by using PmPV **8** in D_2O.

UV-vis-NIR absorption spectra of the supernatant solution provided consistent evidence that the polymer selectively enriched (7,5), (6,5), (8,4) SWNTs (Figure 6). Clearly the water soluble PmPV **8** exhibited notable selectivity toward the SWNTs of small diameters. Interestingly, the sample of SWNT/(PmPV **8**) was depleted of the (13,4) SWNT (see Figure 3a), in contrary to PmPV **7** which slightly enriches (13,4).[21] Drastic difference in the observed selectivity pattern demonstrates the great potential to achieve SWNT separation via control of the polymer conformation.

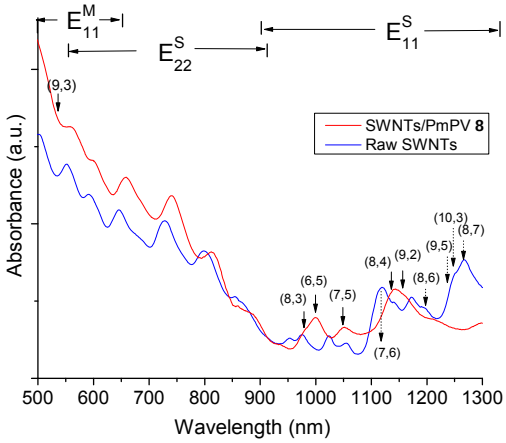

Fig. 6. UV-vis-NIR absorption spectra of PmPV **8**/SWNTs in water. Raw SWNTs were dispersed in sodium dodecyl-benzene sulfonate (SDBS) surfactant.

Different SWNTs present in the raw sample are summarized in Table 1, along with their respective tube diameters. On the basis of the observed selectivity toward (6,5), (7,5) and (9,3) SWNTs, PmPV **8** appeared to have high tendency to host the small tube with relative narrow

range of diameters (d=0.757 – 0.84 nm). Meantime, the dispersion of SWNTs/(PmPV **8**) was depleted of the SWNTs with larger diameters such as (10,3), (9,5) and (12,6) (d>0.936 nm). The result was in agreement with the enhanced conformation as shown in **10**, as the inner –OMe groups reduce the cavity size that matches the SWNTs of small diameter.

Table 1. Distribution of HiPco SWNTs structure and diameter in the studied sample.

SWNTs structures	diameters (nm)		SWNTs structures	diameters (nm)
(6,5) (↑)^{b,c}	0.757		(8,6) (↓)^{b,c}	0.966
(8,3) (↑) ^{a,b,c}	0.782		(9,5) (↓)^{b,c}	0.976
(9,2) (↑)^{b,c}	0.806		(12,1) (↓)^{c}	0.995
(7,5) (↑)^{a,b,c}	0.829		(8,7) (↓)^{b,c}	1.032
(9,3) (↑)^{a,c}	0.847		(10,5) (↓)^{c}	1.050
(8,4) (↑)^{b,c}	0.840		(15,0) (↓)^{a}	1.080
(8,5) ^{a}	0.889		(9,7) (↓)^{c}	1.103
(7,6)^{a,c}	0.895		(10,6) (↓)^{c}	1.111
(9,4) (↓) ^{c}	0.916		(14,1) (↓)^{a}	1.153
(10, 3) (↓)^{a,b,c}	0.936		(13,4) (↓)^{a}	1.206
(12,0) (↓)^{a}	0.940		(11,7) (↓)^{a}	1.231

Note: The SWNTs enriched by PmPV **8** are indicated by a up arrows (↑), while those decreaseing SWNTs are indicated by a down arrows (↓). The superscripts ^{a,b,c} denote the supporting evidence for the observed SWNT enrichment: a: Raman; b: UV-NIR; c: 2D-fluroscence.

Proposed polymer wrapping model. The remarkable difference between **7** and **8**, in terms of SWNT selectivity, could be partially rationalized by considering the substituent impact on the polymer conformational cavity. Since both alkoxy groups in PmPV **7** are hydrophobic, π–π interaction with SWNT surface becomes an important factor. The *para*-phenylene in **7** thus can be rotated to adopt the parallel interaction with SWNT surface as shown in the polymer conformation **9** (Figure 1). The assumption is in agreement with the experimental observation that the absorption λ_{max} of **7** in THF was blue-shifted by ~7 nm when forming the polymer/SWNTs dispersion.[25] As a consequence of the parallel alignment of *para*-phenylene to the SWNT surface, the conformational cavity becomes larger. A wide range of conformational

cavity sizes, corresponding to different degrees of *para*-phenylene rotation, permit PmPV **7** to host SWNTs of various diameters. In sharp contrast, PmPV **8** has a strong preference to adopt the conformation **10**, resulting from the strong interaction between water and the hydrophilic substituents. In the conformation **10**, the methoxy groups are forced to point inwards to confine the conformational cavity, while forming a hydrophobic pocket for SWNTs. The molecular modeling by using HyperChem software showed that the conformational cavity of **8** is slightly larger than 1 nm (Figure 7a). Upon inserting the (7,5) SWNT (d=0.83 nm) through the polymer conformational cavity, the cavity became larger in the aqueous solvent, partly due to the rotation of the methoxy groups (Figure 7b). All *para*-phenylene units remain to be perpendicular to the nanotube axis, as the conformational cavity size is adjusted to host the SWNTs of small diameters. It should be noted that the water soluble polymer plays an important role in the diameter-based sorting process. As seen from Figure 7b, the polar groups of PmPV **8** can interact with water molecules, while the inside of the helical conformation forms a hydrophobic cavity. This could create a water pressure to squeeze the polymer conformation, thereby favoring the tube of small diameter such as (6,5) SWNT.

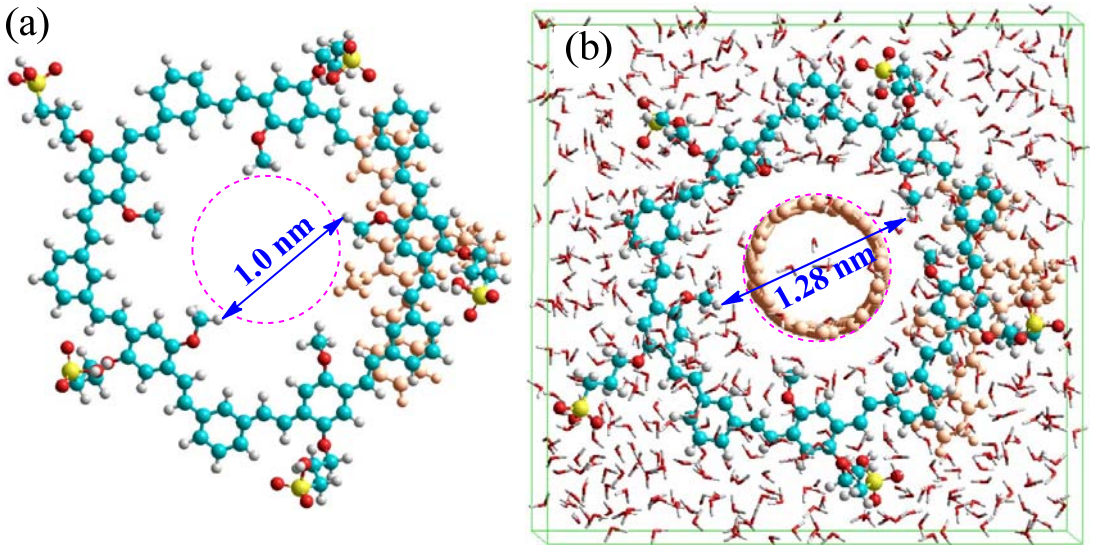

Figure 7. Molecular modeling of PmPV **8** in a helical conformation before (a) and after hosting a (7,5) SWNT (b). The dotted circle (pink color) indicates the approximate perimeter of (7,5) SWNT. For clarity, the (7,5) SWNT and the overlapping phenylenevinylene segment are shown in orange color, and the surrounding water molecules are shown by thin tubes.

2.0 Further Tuning Helical Conformation Cavity by Using Carbon-Carbon Triple Bonds.

As shown in the previous section, the water-soluble P*m*PV **8** showed good selectivity toward the tubes of small diameter. When P*m*PV **8** was used to wrap SWNT, the favorable interaction was to place the *para*-phenylene perpendicular to the tube surface (as shown in **10**, Figure 1). The alternative approach is to align the *para*-phenylene to parallel to SWNT surface (as shown in structure **14**), while maintaining the similar size of the conformational cavity. In order to examine the hypothesis, P*m*PE*p*PE **12** was designed, in which the carbon-carbon triple bonds were used to link the polymer chain to maintain the chain rigidity. In the molecular design, two polar groups were attached on the *para*-phenylene units, in order to promote the parallel alignment of *para*-phenylene along the tube surface. The freely rotating C≡C bond[26] would allow the *para*-phenylene to quickly adopt the favorable interaction with SWNT surface.

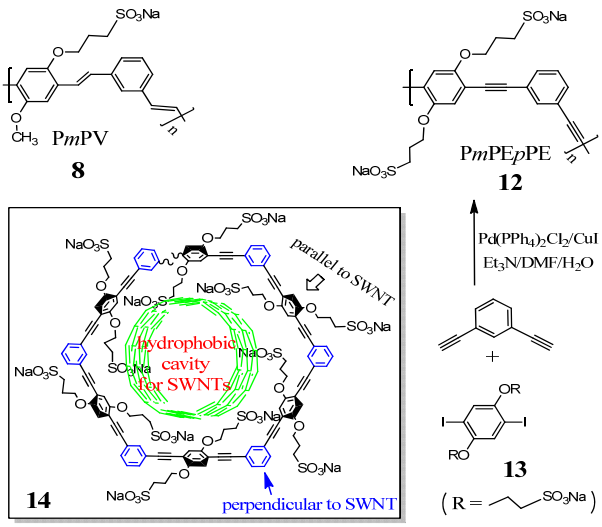

Scheme 2. Synthesis of P*m*PE*p*PE **12**. The structure **14** (inset) illustrates the helical wrapping of **12** on a SWNT.

Results and Discussion

Polymer synthesis and sonication. The polymer **12** was synthesized by Sonogashira coupling of 1,3-diethynylbenzene with 1,4-dialkoxy-2,5-diiodobenzene **13** (Scheme 2),[27] using a similar literature procedure for water soluble PPE.[28] The ^{13}C NMR of P*m*PE*p*PE **12** detected two acetylenic carbons at 92.7 and 83.7 ppm, which matched well with the reported P*m*PE*p*PE structure in literature.[29] In a typical procedure for nanotube dispersion, 3 mg of SWNTs sample were dispersed by using 5 mg of P*m*PE*p*PE in 20 mL deionized water. The solution was sonicated at 0 °C for one and half hours, followed by centrifugation at 7000 rpm for two hours to remove the sediment of the undispersed SWNTs. In order to further remove the catalyst metal and the aggregation of wrapped SWNTs, the supernatant solution was further centrifuged at 20000 rpm twice for two hours.

SWNTs dispersion characterization. AFM image revealed that the SWNTs in the dispersion were in single tube (Fig. 8a), indicating that polymer **12** was an effective dispersing reagent. 2D photoluminescence (PL) maps of SWNT samples were acquired (Fig. 9), where the chirality of SWNTs was assigned according to literature.[24] The intensity of PL peaks for small diameter nanotubes (6,5) and (8,3) (d=0.757 and 0.782 nm, respectively) were increased after dispersion by using polymer **12**. Meanwhile, the peaks of large nanotubes, such as (8,6), (9,5), and (8,7) (d=0.966-1.032 nm), were removed (Fig. 9b). The SWNT (7,5), (8,4), and (7,6) (d=0.829, 0.840, and 0.895 nm, respectively) were found with lower intensity. The changes in PL intensity clearly indicate a narrow diameter selectivity when using polymer **12** in dispersing SWNTs. The discrimination between (8,3) and (8,4) SWNTs, which have a close chiral angel (with merely 0.06 nm difference in diameter), demonstrates the remarkable diameter selectivity of PPE **12**.

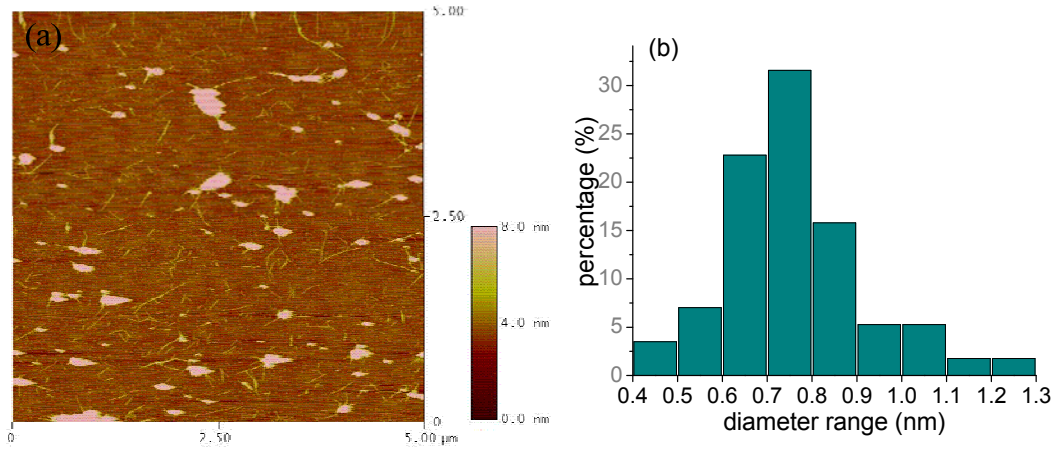

Figure 8. AFM image of SWNTs dispersed with polymer **12** in water (a), and distribution of tube diameters based on the measurement by using tapping mode (b).

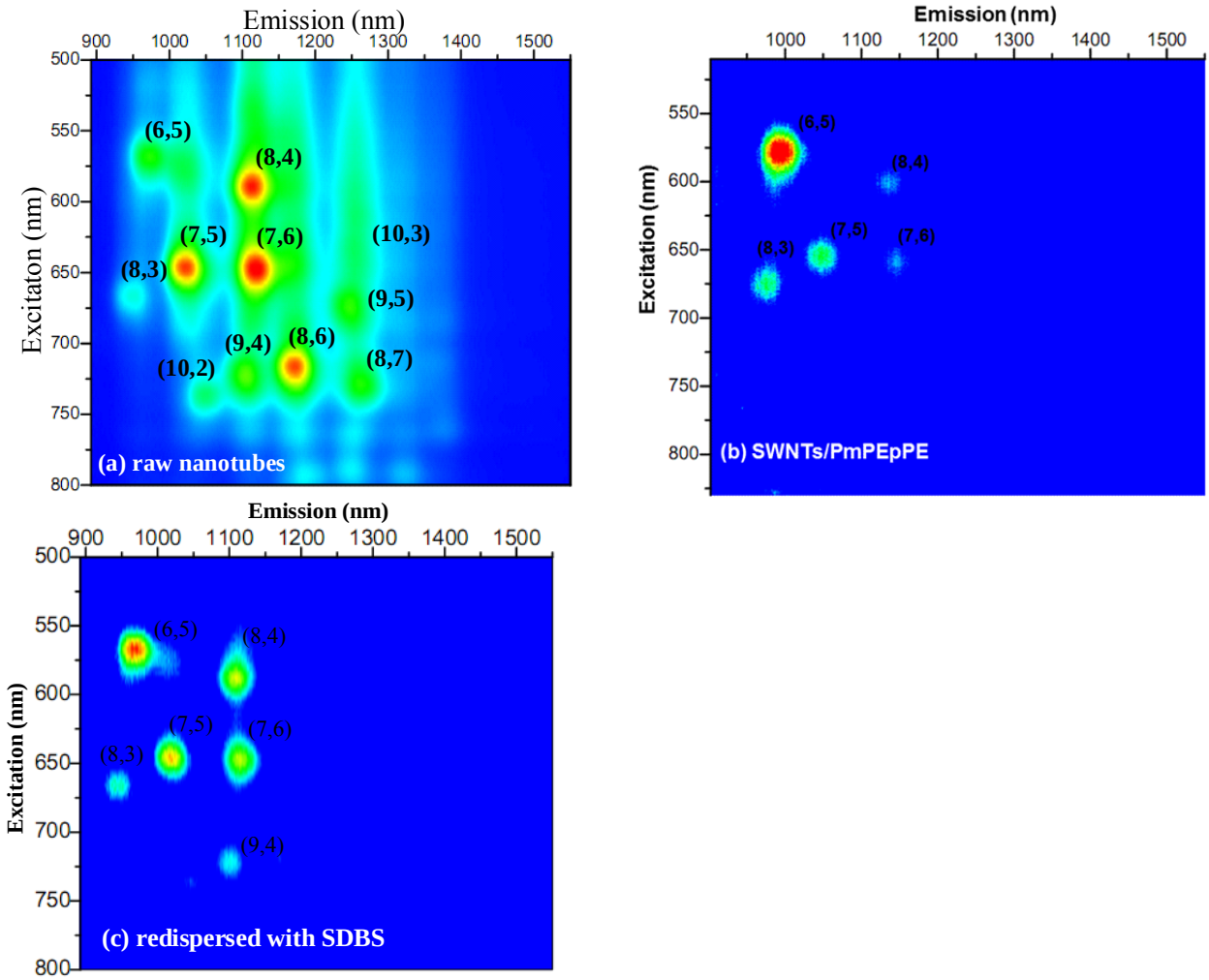

Figure 9. 2D photoluminescence (PL) map of SWNTs, where each SWNT is indicated by its chiral indices (*n*,*m*). (a) Raw SWNTs were dispersed with sodium dodecylbenzenesulfonate (SDBS) surfactant in D_2O. (b) SWNTs were dispersed by using P*m*PE*p*PE in D_2O. Chiral indices (*n*,*m*) of each SWNTs are shown. (c) the P*m*PE*p*PE-dispersed sample was redispersed with SDBS to replace the polymer.

The UV-NIR absorption spectra of the supernatant solution provided consistent evidence (Figure 10). Dispersion by P*m*PE*p*PE **12** enriched small diameter SWNTs (8,3) and (6,5), while discarding larger diameter (8,4) and (7,6) SWNTs. The population of tube (7,5) became relatively low, in agreement with the observation from the 2D fluorescence (Figure 9). The absorption peaks of SWNTs appeared to be broad, as a consequence of interaction between SWNT and wrapping polymer. Although the dispersion in DMSO revealed the more clear

absorption of (6,5) SWNT , the water appeared to be a better solvent since the dispersion in DMSO could not effectively remove (7,5) SWNT.

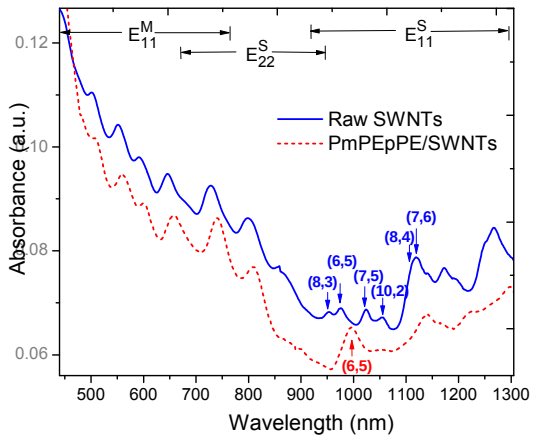

Figure 10. Absorption spectra of SWCNTs dispersed in surfactant SDBS and P*m*PE*p*PE **12**. The supernatant solution of P*m*PE*p*PE/SWNTs was obtained after subjecting to high speed centrifugation.

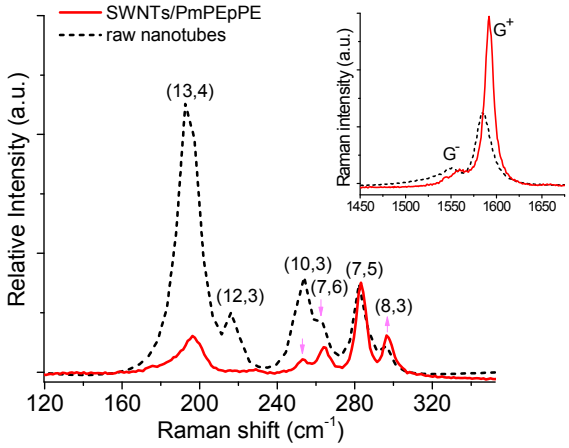

Figure 11. Raman spectra of raw nanotube and SWNTs/P*m*PE*p*PE dispersion in the radial breathing mode (RBM) region (excitation at 647 nm). The inset is the G-band region.

The RBM and G-band regions of Raman spectra further confirmed the nanotube's population changes before and after dispersing by P*m*PE*p*PE (Figure 11). The (7,5) SWNT was chosen as a reference for the tube population change, because the (6,5) SWNT was not observable under the laser frequency used in the Raman.[30] The result indicated that the content of (8,3) was slightly increased in comparison with (7,5), while that of (7,6) and (10,3) was decreased. The relative content of each peak in Raman spectra was measured by comparing the ratio of their integrated

intensity (peaks were approximated by Lorentzian) to that of (7,5).[27] The result clearly indicated that the P*m*PE*p*PE selectively enriched small diameter nanotube (8,3) (0.782 nm),[24] while the nanotubes with larger diameter (d > 0.829 nm) [24] were deselected. In addition, Raman G-band (inset in Figure 11) indicated the enrichment of semiconducting nanotube, which was in agreement with rejection of large diameter metallic (13,4) and (12,3) tubes in RBM region. In other words, dispersion by using P*m*PE*p*PE could be an effective strategy to purify the small diameter semiconducting SWNTs in aqueous media.

As shown in **14** (Scheme 2), the *para*-phenylene segments of P*m*PE*p*PE were aligned in parallel to SWNT's surface, which could induce orbital interaction to affect nanotubes' optical response. In order to examine the effect of the dispersing polymer on fluorescence response, the isolated SWNTs/P*m*PE*p*PE was sonicated in the presence of SDBS to replace the nanotubes from the wrapping polymer: SWNTs/P*m*PE*p*PE + SDBS → SWNTs/SDBS + P*m*PE*p*PE. The fluorescence of the SWNTs/P*m*PE*p*PE and SWNTs/SDBS (Figures 9b & 9c) are summarized in Table 2. The wrapping polymer induced a small spectral shift in emission wavelength ($\Delta\lambda_{em} \approx$ 20-30 nm), due to the π-π interaction between the tube and wrapping polymer chains. In Figure 9c, the signal from (6,5) SWNT remained to be the most intense one. Direct comparison between Figures 9a and 9c thus further confirmed the polymer's selectivity toward (6,5) SWNT. The Raman peaks of the SWNTs in SDBS, however, were only increased by 2-3 wavenumber in comparison with that of SWNTs/P*m*PE*p*PE. The observed Raman peak shift might result from the tube's breathing mode, which was hindered when a large amount of SDBS molecules were accumulated on the surface of a SWNT.

Table 2. Fluorescence of different chiral SWNT in P*m*PE*p*PE and in SDBS.

(n,m)	Purified SWNTs/P*m*PE*p*PE		Purified SWNTs/SDBS [a]		$\Delta\lambda_{em}$ (nm) [c]
	Excitation (nm)	Emission (nm) [b]	Excitation (nm)	Emission (nm) [b]	
(6,5)	577	993	566	973	20
(8,3)	675	975	665	945	30
(7,5)	654	1049	645	1020	29
(7,6)	657	1145	646	1115	30
(8,3)	599	1136	587	1110	26

[a] The sample is prepared by redispersing SWNT/P*m*PE*p*PE in SDBS.
[b] emission reliable range: ±3 nm.

[c] the emission wavelength difference between purified SWNT/P*m*PE*p*PE and purified SWNT/SDBS.

All spectroscopic evidences consistently pointed to that P*m*PE*p*PE **12** exhibits good selectivity toward the small diameter SWNTs (6,5) (Figure 12). The conclusion of enriching (6,5) SWNT was consistent with the tube population observed in AFM (Figure 8b), where most tubes have the diameter between 0.7–0.8 nm. While the helical conformational cavity of **12** could play some role, the diameter-selection mechanism by using polymer conformation alone could not explain the differentiation of SWCNTs of very close diameters.[22] On the basis of fluorescence and Raman intensity (Figures 8 & 9), the polymer's selectivity to (6,5) was slightly higher than (or at least equal) to (8,3), which in turn was higher than to (7,5). The polymer's ability to differentiate SWNTs of close diameter, such as the (6,5) (d=0.757) from (8,3) (d=0.782 nm), (9,2) (d=0.806 nm) and (7,5) (d=0.829 nm), strongly suggests that the observed selectivity involved the electronic interaction between the wrapping polymer and SWNTs.

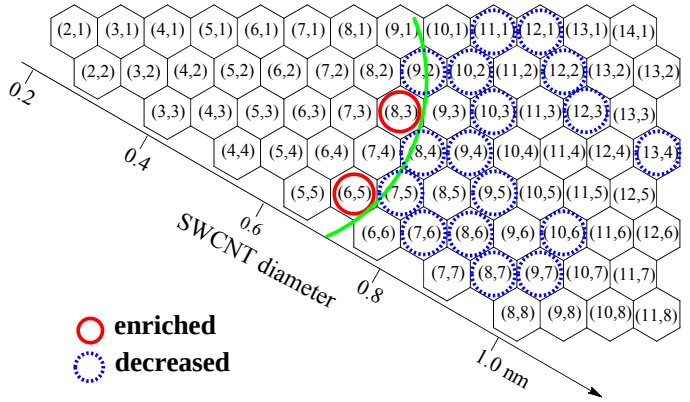

Figure 12. Chirality maps of SWNTs showing that small diameter nanotubes (red bold circle) were enriched by PPE wrapping, and the large diameter nanotube (dotted blue circle) were decreased.

Computational Analysis of Molecular Interaction. In order to shed some light on the intriguing selectivity process, the polymer-SWNT interaction was investigated by using empirical force-field based molecular dynamics and dispersion-corrected density-functional calculations. A detailed molecular dynamics simulation study confirmed that the polymer **12** readily wraps around the SWNTs. The helical conformation of **12** provided a natural helical

cavity that hosts the SWNT of a suitable diameter for intimate orbital interaction (Figure 13, and structure **14** in Scheme 2).

To examine the polymer's affinity to different SWNTs, dispersion-corrected density-functional theory was employed to gain further insight into the polymer-nanotube interaction mechanism. The binding energy was calculated from the first-principles calculations for optimized composite and separate structures of nanotube and polymer **12**: $E = E_{\mathbf{12}/\mathrm{SWNT}} - E_{\mathrm{SWNT}} - E_{\mathbf{12}}$, where $E_{\mathbf{12}/\mathrm{SWNT}}$ is the total energy of the composite, E_{SWNT} is the energy of the nanotube without polymer wrapping, and $E_{\mathbf{12}}$ is the energy of the polymer **12** without the nanotube. In other words, the binding energy can be calculated as the difference between the energy of optimized composite structure and the energy of separated nanotube and polymer **12**. The result shows that the polymer-nanotube complex **12**/(6,5) has a binding energy of –2.989 eV, which is stronger than the nanotube complexes **12**/(6,6) and **12**/(7,5) (binding energies –2.914 and –2.974 eV respectively).

The calculated interaction between polymer **12** and graphene revealed that the PPE backbone acts as charge donor, while the side chain sulfonyl group acts as charge acceptor. The extracted charge density of HOMO-and LUMO-derived bands was shown in Figure 13, revealing the enhanced interaction between polymer **12** and (6.5) SWNT. The extracted binding energy for (6,5), (6,6), and (7,5) demonstrated that (i) the smaller diameter (6,5) was energetically preferred over the slightly larger semiconducting (7,5) tube (by 0.015 eV per phenyleneethynylene (PE) unit), and (ii) for metallic (6,6) and semiconducting (7,5) tubes with virtually the same diameter, the semiconducting tube was energetically preferred (by 0.060 eV per PE unit). These results support the experimental findings that the metallic tubes were deselected as compared to the semiconducting tubes, while the smaller semiconducting (6,5) tube was favored over other semiconducting tubes.

The observed selectivity of semiconducting tubes over the metallic ones was attributed to the differences in the hybridization of HOMO and LUMO-derived bands of polymer **12**.[31,6,32] As seen from Figure 13, the HOMO-derived band from semiconducting tubes displayed much stronger hybridization than that from the metallic counterpart. On the other hand, for the LUMO-derived bands, (6,5) showed stronger hybridization than (7,5), which was attributed to a quantum registry effect in that the band gap of (6,5) matched better with the HOMO-LUMO gap of about 1 eV for polymer **12**.[31,6]

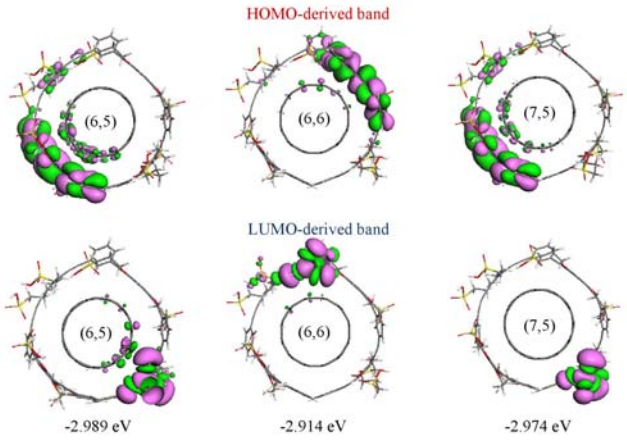

Figure 13. Extracted charge density of HOMO- and LUMO-derived bands of polymer **12** helically wrapped on (6,5), (6,6), and (7,5) SWNTs, respectively. The pink and green colors represent the positive and negative components of the wave function, respectively.

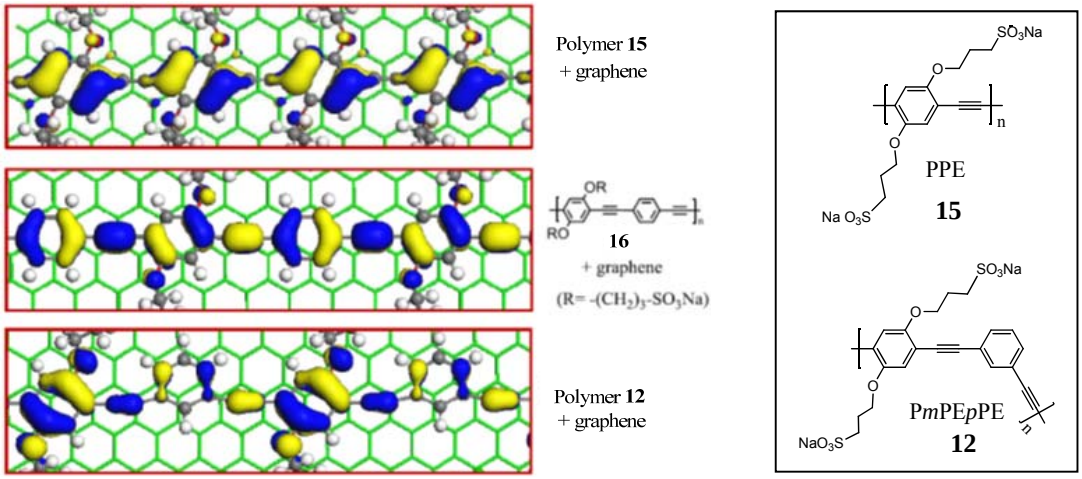

Figure 14. Charge density plots of HOMO- derived bands of polymers **12**, **15**, and **16** on graphene. The wave-function components are distinguished with blue and yellow colors, respectively.

In comparison with **12**, the polymer **15** of linear geometry also forms the donor-acceptor complex resulting in enhanced interactions with graphene or carbon nanotubes.[32] However, the charge density distributions reveals distinctive electron donating behavior between polymers **15** and **12**. Specifically, the charge density of the highest-occupied molecular orbitals (HOMO) is confined at the 1-4 benzene rings of polymer **12**, in sharp contrast to the uniformly distributed electron donating contributions in polymer **15** (Figure 14). Polymer **12** thus exhibits a distinct

advantage in selective dispersion of SWNTs, because the presence of *meta*-phenylene unit provides *not only* a desirable bent angle for the flexible helical wrapping, *but also* a segmented charge transfer for ensuing donor-acceptor interactions.

Conclusion

In conclusion, a water soluble polymer P*m*PE*p*PE was synthesized, in which the *meta*-phenylene unit introduced a bent angle along the polymer backbone to facilitate the helical conformation. In aqueous solution, the polymer was found to disperse SWNTs with good selectivity toward the (6,5) and some selectivity toward (8,3) SWNTs (see Figure 9), which have the small diameters (d=0.757 and 0.782 nm, respectively). The intriguing selectivity was partly due to the helical conformation of polymer backbone, whose cavity size could act as pre-sort mechanism to select the tubes of small diameters (Figure 12). The SWNTs of similar diameters were further differentiated by interaction with the local phenyleneethynylene (PE) chromophores, whose assembly was guided by the helical conformation and assisted by the low rotational barrier of C≡C bonds. Selective dispersion of small diameter (6,5) SWNT illustrated that the synergistic effect of the quantum registry and the helical conformation cavity could be an effective tool to aid the SWNTs sorting. Clearly, the P*m*PE*p*PE **12** was superior to its vinylene analogue **8** in terms of selective SWNT dispersion,[22] as the *para*-phenylenevinylene unit in **12** was aligned parallel to SWNT surface (in contrast to the perpendicular alignment in **8**, see structure **10** in Figure 1 and structure **14** in Scheme 2). Integration of a size control mechanism (via polymer conformation here) with a suitable molecular interaction, therefore, could offer a promising strategy to aid the isolation of a specific SWNT.

3.0 Copolymer of PPV-PPE

It should be noted that most of the selective dispersion by using π-conjugated polymers were carried out in organic solvents (Table 1). As seen in the previous sections, the diameter-based selectivity could be obtained by using poly[(*m*-phenylenevinylene)-*alt*-(*p*-phenylenevinylene)] (P*m*PV) **8** and poly[(*m*-phenyleneethynylene) -*alt*-(*p*-phenylenevinylene)] (P*m*PE*p*PE) **12**, which favored the small diameter tube such as (6,5) SWNT. The aromatic rings along the polymer backbone of P*m*PV **8** are linked by vinylene bonds (–CH=CH–), while that of P*m*PE*p*PE **12** are linked by acetylene bonds (–C≡C–). An interesting question was whether the hybrid polymer PPE-PPV could also exhibit some selectivity.

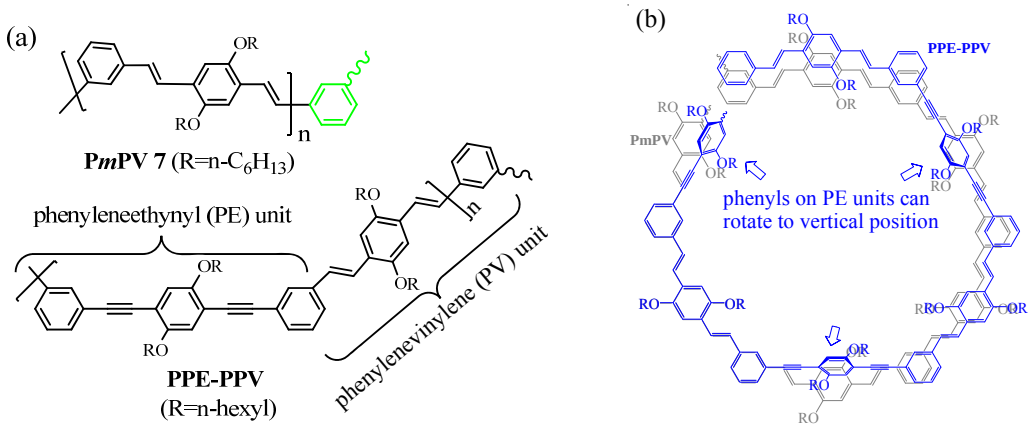

Scheme 3. (a) Chemical structures of P*m*PV and PPE-PPV. (b) Overlay of P*m*PV (grey color) and PPE-PPV (blue color) oligomers in helical conformations, showing that the PPE-PPV has a slightly larger conformation cavity. The thick arrows point to the phenyl groups that can rotate to vertical position.

The PPE-PPV copolymer (Mw ~22,000) was synthesized as described in literature.[33,34] Dispersion of HiPco raw SWNTs was accomplished by sonication, using PPE-PPV at 0°C in THF solvent. Raman analysis of the supernatant revealed that the dispersion enriched SWNTs with a larger diameters, such as (11,7) with d= 1.24 nm (Figure 15a). In addition, PPE-PPV exhibited some notable selectivity towards SWNT (7,5), as the Raman spectra revealed (Figure 15b, excitation at 647 nm).

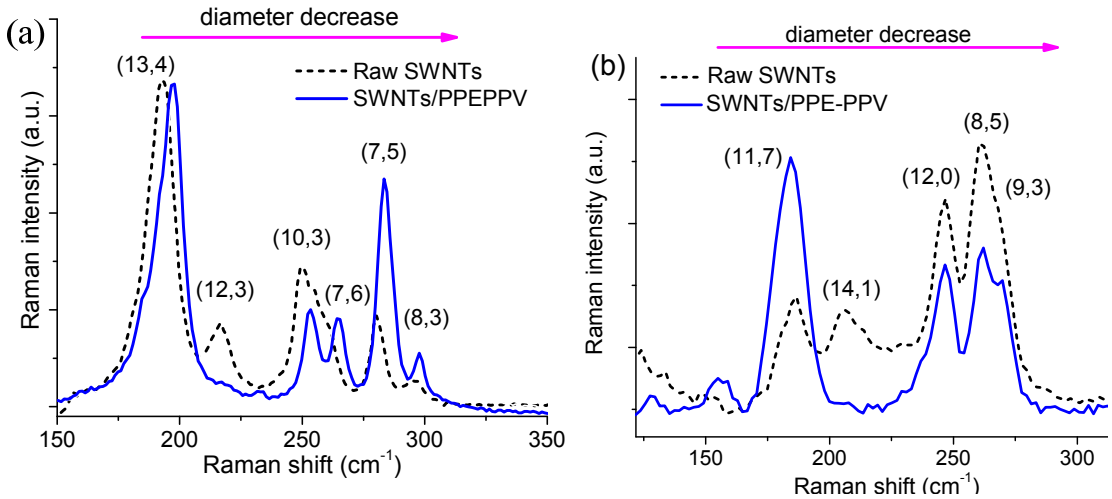

Figure 15. RBM mode of Raman spectra of SWNTs/PPE-PPV in THF when excited at 647 nm (a) and 514 nm (b), respectively. The Raman of raw SWNTs was acquired from its solid.

In comparison with PmPV **7** in THF,[21] PPE-PPV exhibited better selectivity in the same solvent, indicating that the carbon-carbon triple bond (–C≡C–) played a positive role to improve the selectivity. The selectivity of PPE-PPV to SWNTs in THF, however, was relatively poor, in comparison with water-soluble P*m*PV **8** (Figure 3) and P*m*PE*p*PE **12** (Figure 11) in aqueous solution. The observation further confirmed that separation in an aqueous media could have advantages as the hydrophobic cavity of the polymer's conformation could be compressed to enhance the selectivity toward the tubes of the small diameters. In an organic solvent, the polymer backbone would be relatively relaxed, whose relative large conformational cavity might be in favor of a tube of larger diameter as observed from the PPE-PPV copolymer.

3.1 Narrow Distribution of SWNTs by Using Nitric Acid Treatment and Polymer Dispersion

As shown above, the PPE-PPV copolymer exhibited some selectivity toward tubes of relatively large diameter. When coupling with the other methods that could remove the SWNTs of small diameters, it was possible to obtain the enriched sample with few SWNTs of relatively larger diameters. This strategy was illustrated in Scheme 3, where the SWNTs from a HiPco sample were sorted into different groups by their diameters. In the first step, the SWNTs could be presorted by their diameters. And the fraction of the large diameter SWNTs could be further

enriched by PPE-PPV (Step Two) to obtain a sample with narrow chirality distribution (i.e. fewer SWNTs).

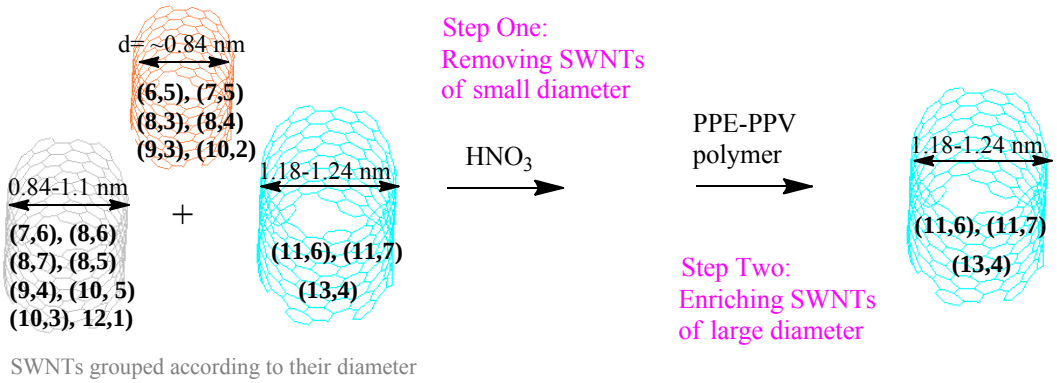

Scheme 3. Schematic illustration to obtain SWNTs of narrow diameter distribution by using a two-step approach.

In collaboration with researchers at NASA Glenn Research Center, a simple chemical process was found to obtain a relatively pure sample. In the first purification step, the raw SWNTs (about 0.5-1 g) prepared from HiPco process were treated with aqueous HNO_3 (2.6 M, 300 mL) under reflux conditions to afford SWNTs **I** in ~30% yield.[21] Interestingly, majority of semiconducting SWNTs, including (10,3), (7,5) and (8,3) species, were removed, as observed from Raman spectra (Figure 16a). UV-vis absorption spectra (Figure 17) further confirmed the Raman observations, since the nitric acid-treated sample SWNTs **I** revealed much lower absorption between 1050-1350 nm which was associated with the semiconducting (7,5) and (8,3) SWNTs.[7] The nitric acid treatment, therefore, selectively removed the SWNTs of smaller diameter: (8,3), (7,5) and (10,3) SWNTs (d=0.78, 0.83 and 0.93 nm, respectively).[21,24] The metallic (12,3) and (13,4) SWNTs with respective tube diameter 1.077 and 1.206 nm, however, were not affected. Raman analysis of the sample series with green laser excitation at 514 nm displayed a consistent pattern (Figure 16b), showing that the nitric acid removed the small-diameter (9,3) and (8,5) SWNTs (with diameter 0.84 nm and 0.89 nm, respectively).

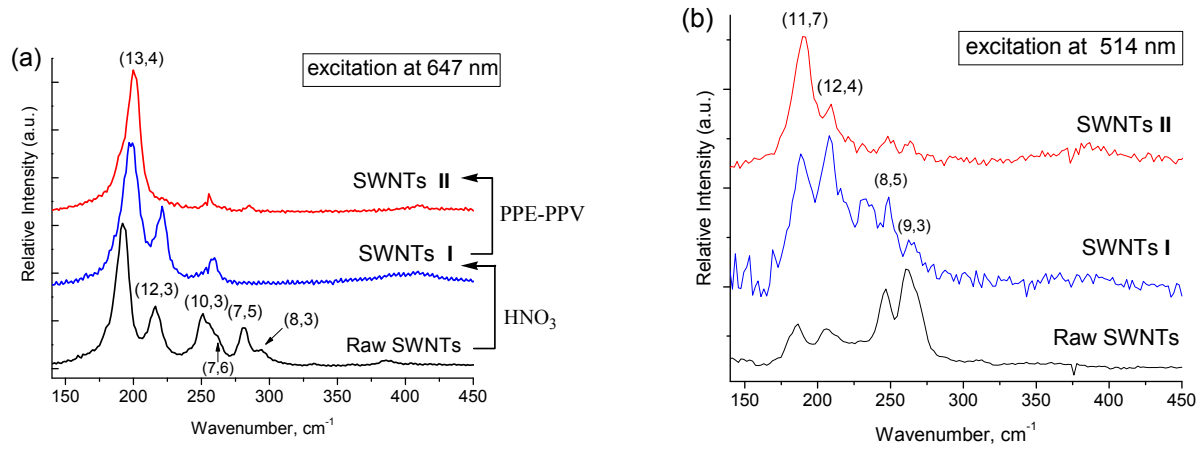

Figure 16. Raman spectra of SWNT samples in radial breathing mode (RBM) region at 647 nm (a) 514 nm excitation (b). The as-prepared raw SWNTs were subsequently treated with HNO_3 (SWNTs **I**) and wrapped by PPE-PPV polymer (SWNTs **II**).

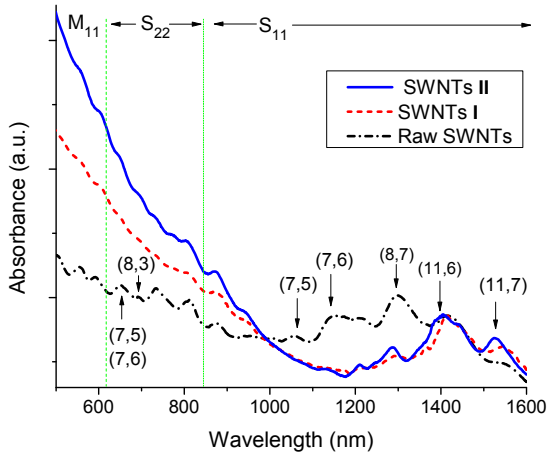

Figure 17. UV-vis absorption spectra of dispersed SWNTs in THF.

High resolution TEM (Figure 18) further revealed that nanotubes in SWNTs **I** were bundled. The tube diameters were found between 1-1.2 nm, in agreement with the observation from Raman spectra. The result was in sharp contrast to using concentrated H_2SO_4/HNO_3 (ratio 1:9, with 97% H_2SO_4 and 60% HNO_3) at room temperature, which was reported to selectively react with *metallic* SWNTs of smaller diameter (less than 1.1 nm).[35] A possible explanation is that the dilute HNO_3 generated low concentration of NO_2^+, which selectively reacted with the small-diameter SWNTs. The observed higher reactivity of the small-diameter SWNTs could be attributed to their increased curvature strain,[36,37,38] in comparison with the relative lower reactivity of larger diameter nanotubes.

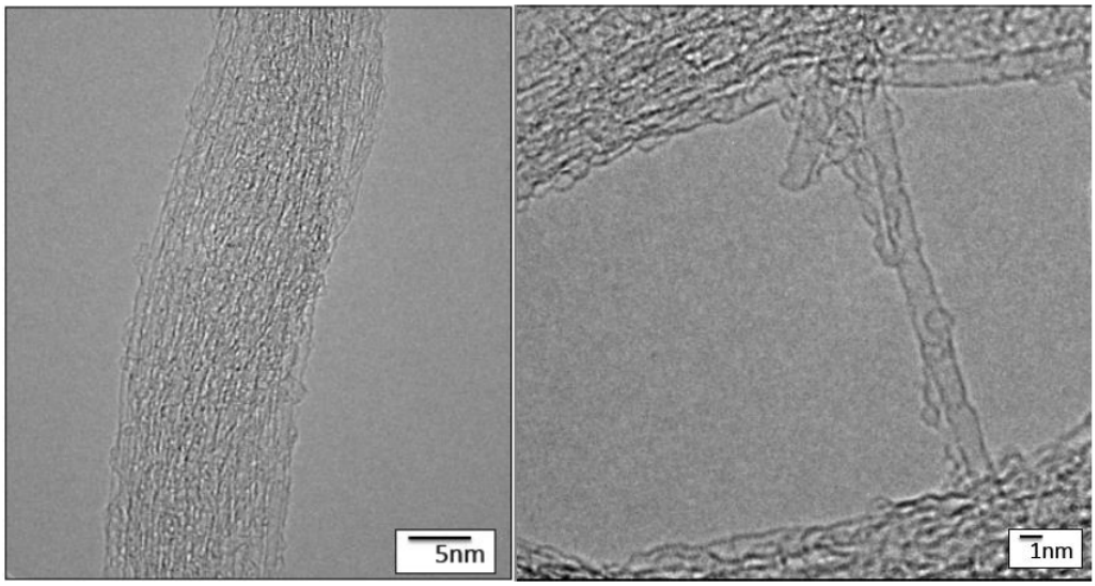

Figure 18. High resolution TEM images of SWNTs **I.** The sample contains bundled SWNTs (left image), and the individual tube (right image).

The intriguing chemical selectivity of HNO_3 toward different (n,m) SWNTs was further examined by photoluminescence (PL) spectra. Figure 19 showed the 2D-PL mapping of the dissolved SWNTs in THF, where the SWNTs were assigned according to literature.[24] Nitric acid treatment removed nearly all the small diameter tubes (d<0.9 nm, see Table 3), including the major semiconducting species (8,4) and (7,6) SWNTs. The result complements the finding from the Raman spectra (Figure 16), demonstrating that the nitric acid selectively reacted with both semiconducting and metallic SWNTs of small diameters.

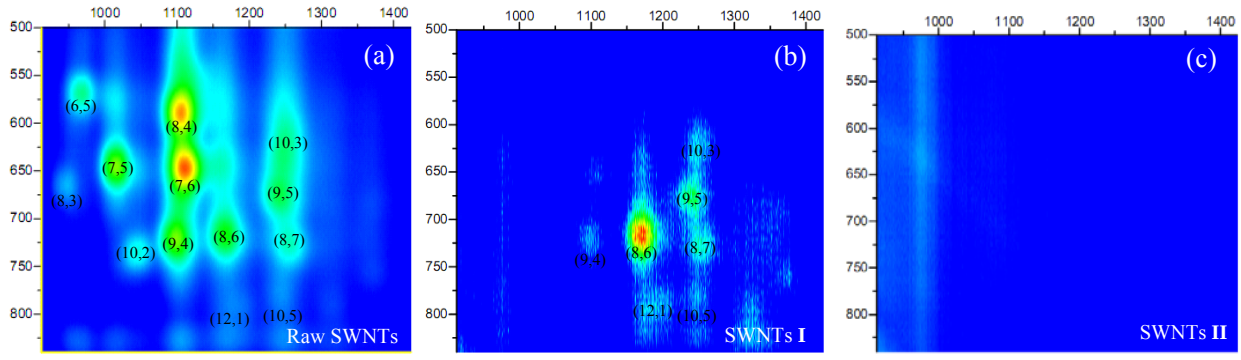

Figure 19. 2D photoluminescence (PL) of SWNTs samples in THF (excitation: 500-840 nm; emission: 912-1415 nm). Raw SWNTs was dispersed with addition of sodium dodecylbenzene sulfonate (SDBS) surfactant (65% in water).

Selective polymer dispersion. The SWNTs **I** were then treated with PPE-PPV (M_w=31,000, PDI=4.6) which was synthesized as described previously.[33] In a typical dispersion procedure,[21] 3 mg of SWNTs **I** sample and 20 mL of THF was sonicated for 3 hours. Then 50 μL of PPE-PPV in THF solution (concn = 26.2 mg/mL) was added to the SWNTs suspension, and the mixture was sonicated at 0°C for an additional 1 hour. The supernatant solution was separated from the sediment by centrifugation at 7000 g. Raman analysis of the resulting supernatant solution showed that the (13,4) and (11,7) in SWNTs **I** were separated from the (12,3) SWNT (Figure 16). The sediment sample was found to contain enriched (12,3) SWNT, further confirming the separation. The enriched (11,7) SWNT was also observable from the absorption spectrum (λ_{max} at ~1525 nm, Figure 17), where the absorption peak was assigned according to the literature.[24,39] The absorption band at ~1397 nm, which was assigned to (11,6) SWNT (d=1.186 nm),[24] was relatively less affected. 2D fluorescence spectra (Figure 19b-c) revealed that PPE-PPV treatment further purified the sample by selectively removing (8,6) SWNT. Due to the instrument limitation, we were not able to detect the (11,7) SWNT from the fluorescence spectrum, since its emission is at ~1520 nm (out of the instrument scan range). The results revealed a striking pattern that the reported approach led to a SWNTs sample with very narrow distribution of diameter, which is 1.24 nm and 1.20 nm for (11,7) and (13,4) SWNTs, respectively. Therefore, the combination of the treatment by nitric acid, followed by dispersion with PPE-PPV, provided an effective approach to obtain the sample that was mainly consisting of (13,4) and (11,7).

Raman analysis further revealed that the chemical reaction increased the intensity of D-band due to the reaction on the nanotubes, and decreased the intensity for tangential mode (G-band) due to loss of electronic resonance (Figure 20). Polymer treatment by using PPE-PPV, however, removed those defective tubes of smaller diameters. The result showed that the polymer wrapping was a necessary step in achieving the desirable separation and removing those defective tubes.

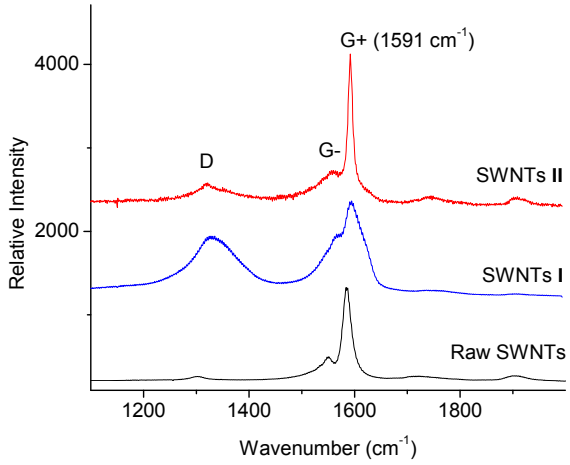

Figure 20. Raman spectra of SWNT samples in tangential mode (G-band) and disorder-related mode (D-band) at 647 nm excitation). The as-prepared raw SWNTs were subsequently treated with HNO_3 (SWNTs **I**) and wrapped by PPE-PPV polymer (SWNTs **II**).

Table 3. Distribution of HiPco SWNTs structure and diameter in the studied sample.

SWNTs structures	Tube diameters (nm)		SWNTs structures	Tube diameters (nm)
(6,5)-*sc*[a]	0.757		(10, 3)-*sc*	0.936
(8,3)-*sc*	0.782		(8,6)-*sc*	0.966
(7,5)-*sc*	0.829		(9,5)-*sc*	0.976
(9,3)-*met*[b]	0.84		(8,7)-*sc*	1.032
(8,4)-*sc*	0.840		(12,3)-*met*	1.077
(8,5)-*met*	0.89		(9,7)-*sc*	1.103
(10,2)-*sc*	0.884		(12,4)-*sc*	1.145
(7,6)-*sc*	0.895		(11,6)-*sc*	1.186
(9,4)-*sc*	0.916		(13,4)-*met*	1.206
			(11,7)-*sc*	1.248

[a,b] the "*sc*" and "*met*"denote *semiconducting* and *metallic* tubes, respectively.

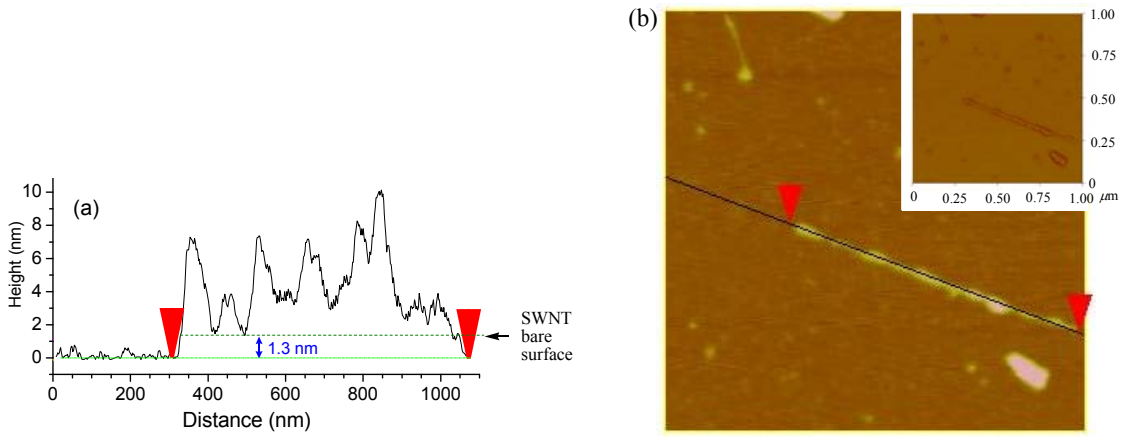

Figure 21. AFM images obtained in tapping mode. (a) A profile along an individual SWNT, where the dashed line shows the 1.3 nm height. (b) Surface images of the SWNT, where the black line indicates the cross-section direction along the tube. The inset image shows the dimension of the same SWNT.

An atomic force microscopy (AFM) image of the SWNT/PPE-PPV sample from the supernatant solution revealed that the SWNT sample was dispersed as single tube (Figure 5). AFM profilometry (in tapping mode) along the lengthwise SWNT direction gave a height profile of regular pattern, indicating that the nanotube was wrapped section by section with multiple polymers chains. From the minimum height of the profile, the diameter of the wrapped nanotube was estimated to be ~1.3 nm, which was in agreement with the diameter of ~1.2 nm reported for (13, 4) and (11,7) SWNTs.

The observed narrow selectivity toward the (13,4) and (11,7) SWNTs could be related to the polymer's ability to adopt a suitable helical conformation for intimate polymer interaction with larger-diameter nanotubes. Molecular modeling study showed that the phenyl rings in the phenyleneethynylene (PE) segments could be rotated easily around the –C≡C– bond due to its low rotational energy barrier.[31,32] As a consequence, the phenyl rings in the PE segments can adopt the parallel alignment along the nanotube surface (Figure 22), thereby resulting in a more favorable π-π interaction. The modeling results also showed that the natural conformational cavity from PPE-PPV was sufficiently large to match the size of (13, 4). The results were consistent with the observations that the PPE-PPV had favorable interaction with large diameter

tubes (13,4) and (11,7) (see Raman spectra in Figure 15), since those tubes with smaller diameters (d<1.14 nm) would be too loosely fitted into the conformational cavity. The ability of PPE-PPV to adopt a natural helical conformation with enhanced parallel π-π interaction for SWNT, in addition to proper diameter match, was thought to play a crucial role in the observed selectivity. The assumption was consistent with the finding that the polymer-dispersed SWNTs were in an individual tube (see AFM in Figure 21).

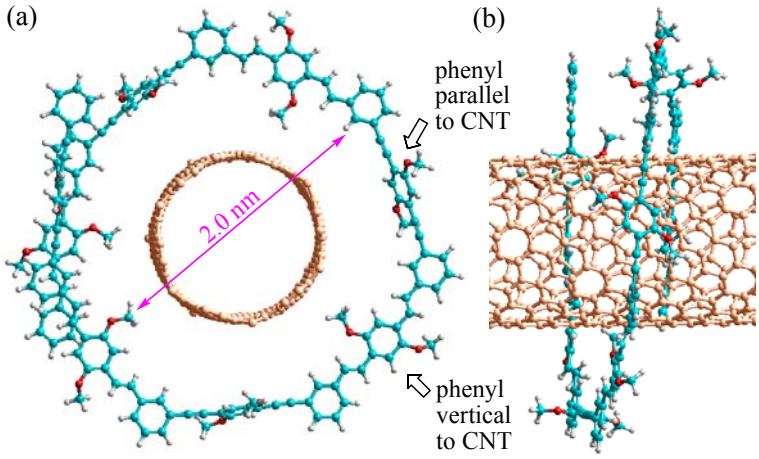

Figure 22. Molecular modeling of PPE-PPV tetramer (n=4) in front (a) and side view (b), showing a helical conformation with proper cavity size (~2.0 nm) to host (13,4) SWNT. For clarity, the tube is shown in orange color.

In summary, we have demonstrated that a narrow diameter range of SWNTs, i.e. (13,4) and (11,7) (d=1.23-1.24 nm), could be isolated by using a sequential treatment with nitric acid, followed by PPE-PPV polymer dispersion. The nitric acid selectively removed the tubes with small diameters, while the dispersion by using PPE-PPV in THF further enriched the tube of relative large diameters. The polymer's selectivity toward the larger tubes was associated with its ability to form a unique helical conformation around the SWNTs. The overall diameter-based sorting process was summarized into Figure 23, where the (n,m) SWNTs in the sample are circled. Nitric acid removed the small diameter tubes (yellow color) selectively, while the remaining SWNTs are sorted into two groups (green and blue colors).

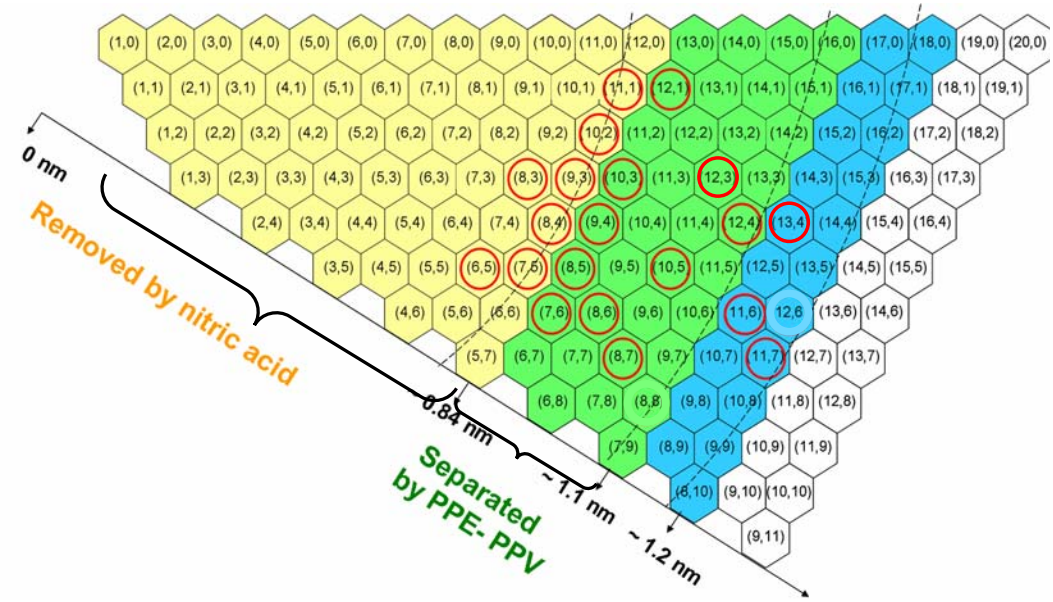

Figure 23. Chality maps of SWNTs showing that small diameter tubes (yellow color) were removed by HNO_3. And the remaining SWNTs (green and blue colors) were sorted by PPE-PPV wrapping.

It should also be noted that the "nitric acid and PPE-PPV" method separated the largest tubes in the HiPco sample (*see* (13,4) and (11,7) in Table 3), while the water soluble polymer P*m*PE*p*PE **12** could be used to enrich (6,5) SWNT (the smallest tube in HiPco sample). The results clearly demonstrated that the cavity of the polymer's natural helical conformation could be tailored to match the diameter of SWNTs, thereby facilitating their separation. The SWNTs could then be released from the wrapping polymer after purification, thereby leading to a useful strategy to access SWNTs of specific diameters for material property studies.

4.0 Separation of Metallic SWNTs by Using Poly(ethyleneimine)

Over the past few years, few strategies have been found to achieve the separation of *met*-SWNTs from *semi*-SWNTs, which include dielectrophoresis,[40] density gradient ultracentrifugation,[41,42] gel electrophoresis,[43] and single-stranded DNA (ssDNA).[44] All of these methods, however, suffer from either scalability, or poor separation efficiency, or both. The challenge remains in searching for an effective and simple separation method that has potential to operate on a practical large scale.

Column chromatography is one of the traditional separation methods, which are widely used in the laboratory and drug industry for purification of organic chemicals. Few studies have been reported in developing the chromatographic methods for SWNTs purification. Recently, Moshammer *et al*.[43] successfully separated *met*- and *semi*-SWNTs by using an allyl dextran-based size-exclusion gel. Kataura *et al*.[10] further showed that single-chirality separation of *semi*-SWNTs can be achieved by using an allyl dextran-based gel. Although the gel chromatography can separate *semi*- from *met*-SWNTs, it can not differentiate different *met*-SWNT species.[10] In addition, the gel chromatography[10] requires the use of a sequence of columns, which give the SWNTs in very dilute solution. In order to make the pure SWNT to be accessible in every laboratory, it is desirable to develop a low cost column chromatography, as it involves only a simple experimental set-up. In the effort to search for a column packing materials, we have examined the polyethyleneimine (PEI)-modified cellulose, which could be used for easy separation of the *met*-SWNTs.

The branched polyethyleneimine (PEI) (Mw~600, purchased from Aldrich) was thus used to disperse the HiPco SWNTs in water by sonication at 0 °C for two hours. The resulting dispersion was subjected to centrifugation at 7000 g for two hours, in order to remove the sediment of undispersed SWNTs. Raman spectra of the SWNTs/PEI dispersion (Figure 24) revealed that *semi*-SWNTs were enriched, indicating that PEI exhibited higher affinity to *semi*-SWNTs. The finding was not trivial, as previous studies had shown that a primary amine could exhibit selective affinity toward either metallic[45] or semiconducting SWNTs,[46,47] depending on the specific amine and conditions used. Photoluminescence of SWNTs/PEI further revealed that the polymer was selective toward certain *semi*-SWNTs, including (7,6) and (8,6) SWNTs (Figure 25).

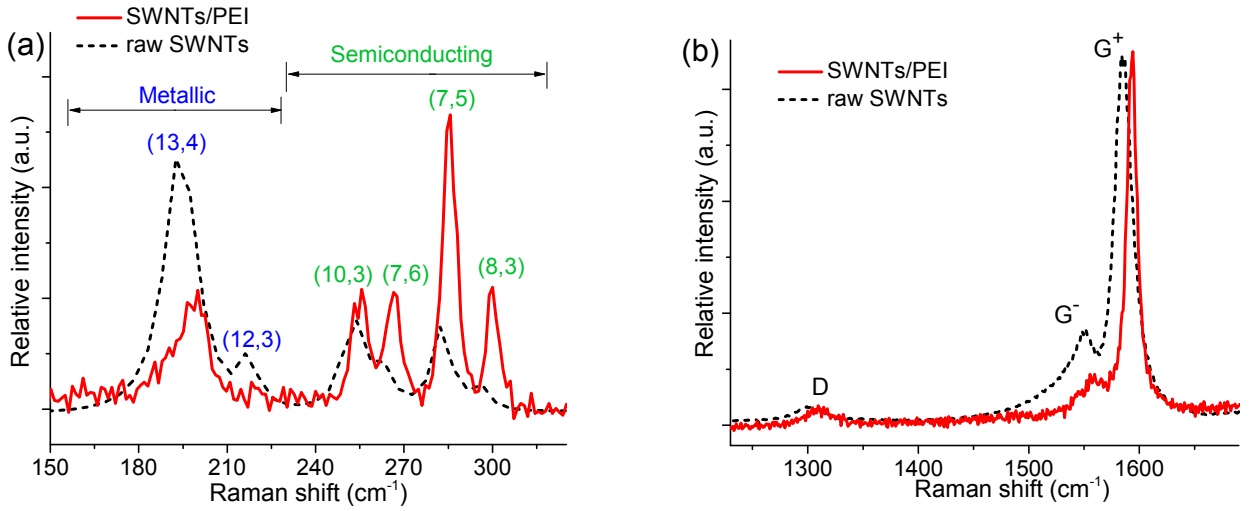

Figure 24. Raman spectra of raw SWNTs and SWNTs/PEI dispersion (excited with 647 nm laser).

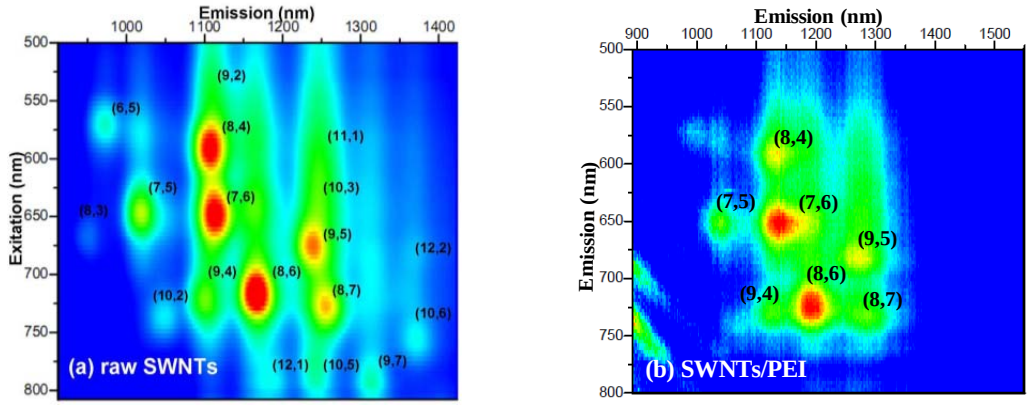

Figure 25. 2D photoluminescence of SWNTs dispersed with SDBS (a) and PEI (b) in D_2O.

Encouraged by the finding that the PEI can selectively disperse *semi*-SWNTs, the PEI was incorporated onto the phosphorylated cellulose which was synthesized by using a literature procedure.[48] In the experiment design, the branched polyethyleneimine (PEI) was absorbed onto a phosphorylated cellulose (Figure 26). While the more basic secondary and tertiary amines could be used for binding with phosphoric groups, the dangling primary amines on PEI were available for interaction with SWNTs. It was assumed that the primary amine groups on the surface of cellulose could interact more strongly with *semi*-SWNTs, thereby retaining the *semi*-SWNTs on the column while allowing the *met*-SWNTs to move out with the mobile phase

(Figure 26). It should be noted that the polymeric amines on PEI have the following advantages over a small molecule amine. First, the polymeric amines can hold the selected SWNTs onto the stationary phase to allow direct separation from those non-selected SWNTs in the mobile phase. Second, when the SWNTs in the mobile phase pass through a stationary phase containing amines, the SWNTs can interact with the dangling amines for multiple times as the tubes are moving through the column, thereby greatly increasing the separation efficiency for different SWNT species.

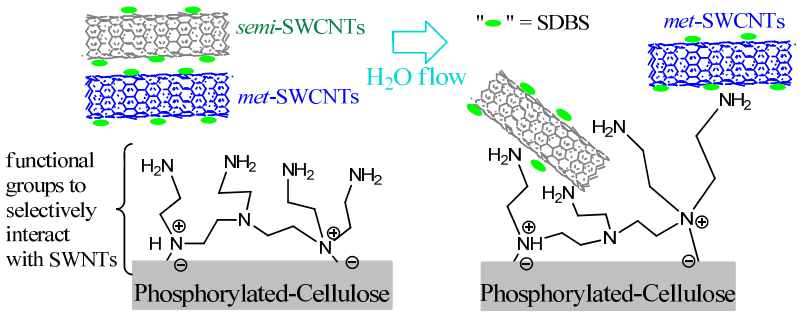

Figure 26. (a) Structure of PEI-cellulose where polyethyleneimine (PEI) is absorbed on the phosphorylated cellulose. (b) and the top section of (a) are schematic illustration of SWNT separation. First, SWNTs dispersed in SDBS surfactant are loaded on the front of PEI column. Second, under the water flow, *met*-SWNTs are moving with the mobile phase while *semi*-SWNTs are holding relatively tight on the column.

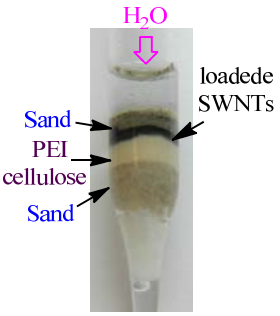

Figure 27. A column packed with PEI and SWNTs for separation.

A sample of raw SWNTs (~3 mg) from HiPco process was dispersed in sodium dodecylbenzene sulfonate (SDBS) (20 mL aqueous solution; concentration: 2.8 mg/mL) by sonication at 0ºC for 1.5 hr. The resulting suspension (3 mL) was then loaded onto a short column packed with the PEI-cellulose in a glass pipette (~5.6 mm ID and ~7 mm OD). When water was used as eluent, excess SDBS was flowing out first (within a few minutes as observed on a UV-vis spectrometer). After pumping water through the column (about 200 mL in about 24-48 hrs), the PEI-cellulose section below the black region was cut out from the column. The separated SWNTs can be released from the PEI-cellulose by adding several drops of HCl solution (0.01 mol/L), then neutralized with NH_4OH. The AFM image (Fig. 28c) revealed that the tubes in the resulting solution were well dispersed and the average length of the isolated

SWNTs were around 300 nm, with diameter being about 1.0-1.3 nm.

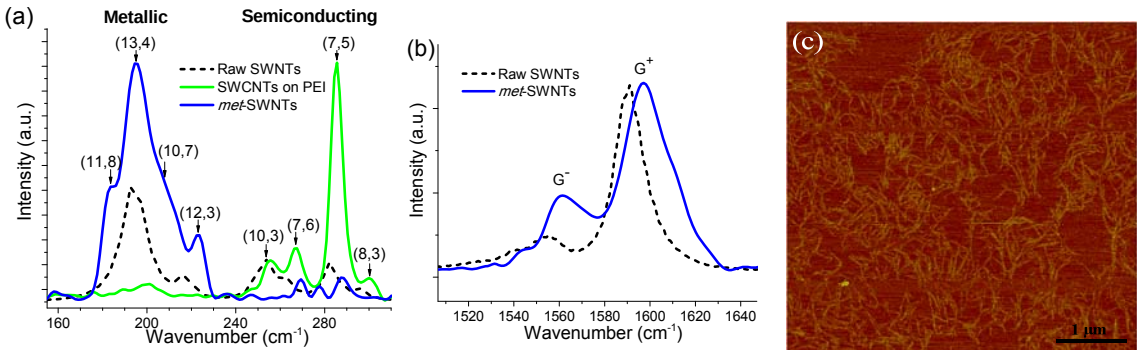

Figure 28. (a) Raman spectra in the radial breathing mode (RBM) region for raw SWNTs, isolated *met*-SWNTs, and residual SWNTs on the top section of PEI-cellulose, with excitation at 647 nm. (b) Raman G-band for raw and *met*-SWNTs. (c) AFM image of the isolated *met*-SWNTs.

Raman spectra were acquired to analyze the chirality composition of SWNTs. On the basis of Raman peak positions,[49] the isolated SWNTs were identified as shown in Figure 28a, which contained about 70% (13,4) SWNT. The Raman G-band of the isolated SWCNTs (acquired from the solid state) revealed moderate increase in the relative intensity of G^- band at ~1560 cm^{-1} (Fig. 28b), in agreement with the increasing metallic SWCNTs. Raman peak assignments for the *met*-SWNTs are summarized in Table 4, which is consistent with the *met*-SWNTs identified in a HiPco sample that contains metallic tube family (2n+m)=27 and (2n+m)=30 (listed in Table 4).[50] It was noted that the Raman peak for tube (12,3) was shifted from 215 cm^{-1} in the raw sample to 223 cm^{-1} in the purified sample (Fig. 28a).

The result showed that the PEI selectively retained *semi*-SWNTs, which explained why metallic nanotubes were slowly moving with the mobile phase while semiconducting SWNTs were held by PEI cellulose. The proposed mechanism

Table 4. Raman Evidence for Enrichment of *met*-SWNTs

	(n,m)	*Lit Raman*[23] (cm^{-1})	*Our Raman* (cm^{-1})
Family 27	(9,9)	192	198.5
	(10,7)	202.5	208
	(11,5)	209.5	--
	(12,3)	215	223
Family 30	(10,10)	172	168
	(11,8)	179.5	183
	(12,6)	189	--
	(13,4)	192	195

was also consistent with the observation that the isolated *met*-SWNTs remained to be soluble in water. Scanning electron microscope (SEM) image further revealed that the surface of PEI-cellulose packing (from the black band in Fig. 27, after elution) was covered by SWNTs, in agreement with the proposed higher affinity of PEI to *semi*-SWNTs (see also Raman spectra in Figure 28a).

It appeared that SWNTs had strong interaction with the amino groups, which led to retention of *semi*-SWNTs on PEI and slow moving of *met*-SWNTs in water mobile phase. It was assumed that the presence of ammonium in the mobile phase could increase its elution strength. When using a dilute ammonium aqueous solution as eluent, different fractions were collected and analyzed (eluent composition shown in Figure 29). UV-vis absorption peak of the eluent revealed notable change for the fractions 1-3 (Figure 30). Interestingly, Raman analysis showed that the first fraction (λ_{max}=633 nm) was predominantly (13,4) SWNT, while the second fraction (λ_{max}=660 nm) and third fraction (λ_{max}=605 nm) were armchair (10,10) and (9,9) SWNT. The isolated armchairs exhibited only G^+ band at ~1600 cm^{-1}, which is similarly observed from the armchair SWNT by using DNA sequence[44] and centrifugation.[51] The results suggest that the PEI column chromatography could separate the different armchair SWNTs from the other *met*-SWNTs (Table 4), although further study is required to further understand the isolation process and its potential.

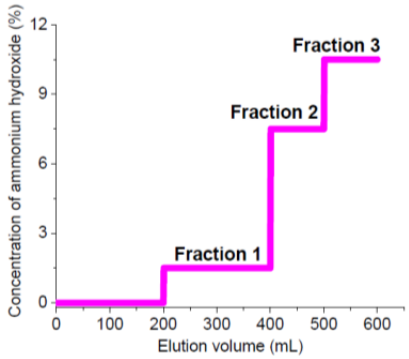

Figure 29. Solvent composition versus elution volume, which is used to obtain SWNT fractions 1-3. The eluent is partially protonated ammonium hydroxide by addition of a small amount of HCl (3%), in which the molar ratio of NH_3 to HCl is 50:1.

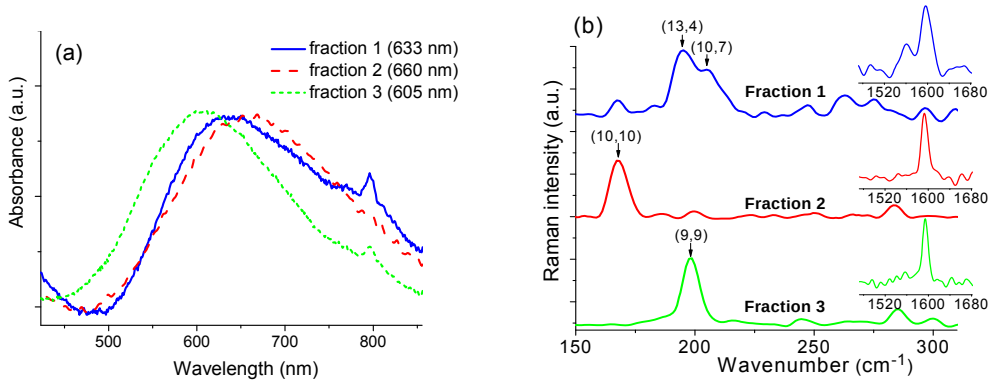

Figure 30. (a) UV-vis-NIR absorption spectra of different fractions by using different concentration of NH_3 aqueous solution as eluent. (b) Raman spectra (RBM) for fractions 1-3, where the inset shows the respective G band (excitation at 647 nm).

In summary, a potential method was identified for isolation of *met*-SWNTs by using PEI column chromatography with aqueous eluent. The Raman RBM and optical absorption data suggest that the isolated SWNTs were enriched *met*-SWNT mainly consisting of (13,4). In addition, the PEI column showed the potential in isolating different armchair SWNT when using ammonium aqueous solution as eluent. Further study should be carried out to optimize the separation efficiency and simplify the operation procedure.

Publications

During the period from June 1, 2010 to May 31, 2013, the following 27 publications have been achieved.

- D. Samarakoon; X.-Q. Wang; Tunable Band Gap in Hydrogenated Bilayer Graphene, ACS NANO **2010**, 7, 4126-4130.
- X.-Q. Wang, Structural and electronic stability of a volleyball-shaped B-80 fullerene, PHYSICAL REVIEW B **2010**, 15, 153409-1-4.
- C. Kah; J. Nathaniel; K. Suggs; et al., Structural and Electronic Stability of Russian-Doll-Structured Sc4C2@C-80, JOURNAL OF PHYSICAL CHEMISTRY C **2010**, 30, 13017-13019.
- J. Yao; Y. Chen; Y. Pang, Application of Sonochemistry in the Isomerization of Carbon-Carbon Double Bonds, JOURNAL OF POLYMER SCIENCE PART A-POLYMER CHEMISTRY **2010**, 22, 5254-5257.
- D. Samarakoon; Z. Chen; C. Nicolas; et al. Structural and Electronic Properties of Fluorographene, SMALL **2011**, 7, 965-969.
- K. Suggs; D. Reuven; X.-Q. Wang, Electronic Properties of Cycloaddition-Functionalized Graphene, JOURNAL OF PHYSICAL CHEMISTRY C **2011**, 8, 3313-3317.
- Y. Xu; A. Malkovskiy; Y.Pang, A graphene binding-promoted fluorescence enhancement for bovine serum albumin recognition, CHEMICAL COMMUNICATIONS **2011**, 23, 6662-6664.
- Y. Xu; M. Guo; X. Li; et al., Formation of linear supramolecular polymers that is based on host-guest assembly in water, CHEMICAL COMMUNICATIONS **2011**, 31, 8883-8885
- Z. Chen; X.-Q. Wang, Stacking-dependent optical spectra and many-electron effects in bilayer graphene. PHYSICAL REVIEW B **2011**, 8, 081405-1-4.
- D. Samarakoon; X.-Q. Wang, Twist-boat conformation in graphene oxides, NANOSCALE **2011**, 1, 192-195.
- K. Suggs; V. Person; X.-Q. Wang, Band engineering of oxygen doped single-walled carbon nanotubes, NANOSCALE **2011**, 6 2465-2468.
- R. Gunasingh; C. Kah; K. Quarles; et al., Dispersion corrections in the boron buckyball and nanotubes, APPLIED PHYSICS LETTERS **2011**, 26.
- K. Quarles; C. Kah; R. Gunasinghe; et al., Filled Pentagons and Electron Counting Rule for Boron Fullerenes, JOURNAL OF CHEMICAL THEORY AND COMPUTATION **2011**, 7, 2017-2020.
- Z. Chen; C. Kah; X.-Q. Wang, Electronic shell structures of Russian-doll-style Sc4C2@C-80, CHEMICAL PHYSICS LETTERS **2011**, 4-6, 230-232.
- Y. Chen; Y. Xu; K.Perry; et al., Achieving Diameter-Selective Separation of Single-Walled Carbon Nanotubes by Using Polymer Conformation-Confined Helical Cavity, ACS MACRO LETTERS **2012**, 6, 701-705 Y. Chen; A. Malkovskiy; X.-Q. Wang; et al., Selection of Single-Walled Carbon Nanotube with Narrow Diameter Distribution by Using a PPE-PPV Copolymer, ACS MACRO LETTERS **2012**, 1, 246-251
- M. Williams; D. Samarakoon; D. Hess; et al., Tunable bands in biased multilayer epitaxial graphene, NANOSCALE **2012**, 9, 2962-2967.

- D. Reuven; K. Suggs; M. Williams; et al., Self-Assembly of Biofunctional Polymer on Graphene Nanoribbons, ACS NANO **2012**, 2, 1011-1017.
- J. Hargrove; H. Shashikala; L. Guerrido; et al., Band gap opening in methane intercalated graphene, NANOSCALE **2012**, 15, 4443-4446.
- D. Samarakoon; X.-Q. Wang, Intrinsic half-metallicity in hydrogenated boron-nitride nanoribbons, APPLIED PHYSICS LETTERS **2012**, 10.
- D. Reuven; H. Li; I. Harruna; et al., Self-assembly of metallopolymer guided by graphene nanoribbons, JOURNAL OF MATERIALS CHEMISTRY **2012**, 31, 15689-15694.
- J. Nathaniel; X.-Q. Wang, Tunable electron and hole doping in FeCl3 intercalated graphene, APPLIED PHYSICS LETTERS **2012**, 21.
- H. Shashikala; C. Nicolas; X.-Q. Wang, Tunable Doping in Graphene by Light-Switchable Molecules, JOURNAL OF PHYSICAL CHEMISTRY C **2012**, 49, 26102-26105.
- O. Ogunro; C. Nicolas; E. Mintz; et al., Band Gap Opening in the Cycloaddition Functionalization of Carbon Nanotubes, ACS MACRO LETTERS **2012**, 4, 524-528.
- Sapkota; M. Roundtree; J. Hall; et al., Tunable band gap in gold intercalated graphene, PHYSICAL CHEMISTRY CHEMICAL PHYSICS **2012**, 46, 15991-15994.
- R. Gunasinghe; D. Reuven; K. Suggs; et al., Filled and Empty Orbital Interactions in a Planar Covalent Organic Framework on Graphene, JOURNAL OF PHYSICAL CHEMISTRY LETTERS, **2012**, 20, 3048-3052
- D. Samarakoon; R. Gunasinghe; X.-Q. Wang, A trigonal planar network in hydrogenated epitaxial graphene: a ferromagnetic semiconductor, JOURNAL OF MATERIALS CHEMISTRY C 2013, 15, 2696-2703.
- Y. Chen; Y. Xu; Q. Wang; et al., Highly Selective Dispersion of Carbon Nanotubes by Using Poly(phenyleneethynylene)-Guided Supermolecular Assembly, SMALL **2013**, 6, 870-875.

Reference List

1. Treacy, M. M. J.; Ebbesen, T. W.; Gibson, J. M. Exceptionally high Young's modulus observed for individual carbon nanotubes. *Nature* **1996,** *381* (6584), 678-680.
2. White, C. T.; Todorov, T. N. Carbon nanotubes as long ballistic conductors. *Nature* **1998,** *398*, 240-242.
3. Ouyang, M.; Huang, J.-L.; Cheung, C. L.; Lieber, C. M. Energy gaps in "metallic" single-walled carbon nanotubes. *Science* **2001,** *292*, 702-705.
4. Meyyappan, M. *Carbon Nanotubes: Science and Applications;* CRC Press: New York, 2005.
5. Komatsu, N.; Wang, F. A Comprehensive Review on Separation Methods and Techniques for Single-Walled Carbon Nanotubes. *Materials* **2010,** *3*, 3818-3844.
6. JU, S. Y.; Doll, J.; Sharma, I.; Papadimitrakopoulos, F. Selection of carbon nanotubes with specific chiralities using helical assemblies of flavin mononucleotide. *Nature Nanotechnology* **2008,** *3*, 356-362.
7. Tu, X.; Manohar, S.; Jagota, A.; Zheng, M. DNA sequence motifs for structure-specific recognition and separation of carbon nanotubes. *Nature* **2009,** *460*, 250-253.
8. Ghosh, S.; Bachilo, S. M.; Weisman, R. B. Advanced Sorting of Single-Walled Carbon Nanotubes by Nonlinear Density Gradient Ultracentrifugation. *Nature Nanotechnology* **2010,** *5*, 443-450.
9. Green, A. A.; Duch, M. C.; Hersam, M. C. Isolation of single-walled carbon nanotube enantiomers by density differentiation. *Nano Research* **2009,** *2*, 69-77.
10. Liu, H.; Nishide, D.; Tanaka, T.; Kataura, H. Large-scale single-chirality separation of single-wall carbon nanotubes by simple gel chromatography. *Nature Communications* **2011,** *2*, 309.
11. Pan, X.; Li, L.-J.; Chan-Park, M. B. Diameter- and Metallicity-Selective Enrichment of Single-Walled Carbon Nanotubes Using Polymethacrylates with Pendant Aromatic Functional Groups. *Small* **2010,** *6*, 1311-1320.
12. Chen, F.; Wang, B.; Chen, Y.; Li, L. J. Toward the Extraction of Single Species of Single-Walled Carbon Nanotubes Using Fluorene-Based Polymers. *Nano Lett.* **2007,** *7*, 3013-3017.

13. Ozawa, H.; Ide, N.; Fujigaya, T.; Niidome, Y.; Nakashima, N. One-pot separation of highly enriched (6,5)-single-walled carbon nanotubes using a fluorene-based copolymer. *Chemistry Letters* **2011,** *40*, 239-241.
14. Berek, D. Size exclusion chromatography - A blessing and a curse of science and technology of synthetic polymers. *Journal of Separation Science* **2010,** *33*, 315-335.
15. Nish, A.; Hwang, J.-Y.; Doig, J.; Nicholas, R. J. Highly selective dispersion of singlewalled carbon nanotubes using aromatic polymers. *Nature Nanotechnology* **2007,** *2*, 640-646.
16. Sturzl, N.; Hennrich, F.; Lebedkin, S.; Kappes, M. M. Near Monochiral Single-Walled Carbon Nanotube Dispersions in Organic Solvents. *J. Phys. Chem. C* **2009,** *113*, 14628-14632.
17. Ozawa, H.; Fujigaya, T.; Niidome, Y.; Hotta, N.; Fujiki, M.; Nakashima, N. Rational Concept To Recognize/Extract Single-Walled Carbon Nanotubes with a Specific Chirality. *J. Am Chem. Soc.* **2011,** *133*, 2651-2657.
18. Tange, M.; Okazaki, T.; Iijima, S. Selective Extraction of Semiconducting Single-Wall Carbon Nanotubes by Poly(9,9-dioctylfluorene-alt-pyridine) for 1.5 ++m Emission. *ACS Applied Materials & Interfaces* **2012,** *4*, 6458-6462.
19. Lee, H. W.; Yoon, Y.; Park, S.; Oh, J. H.; Hong, S.; Liyanage, L. S.; Wang, H.; Morishita, S.; Patil, N.; Park, Y. J.; Park, Y. J.; Spakowitz, A.; Galli, G.; Gygi, F.; Wong, P. H. S.; Tok, J. B. H.; Bao, Z. Selective dispersion of high purity semiconducting single-walled carbon nanotubes with regioregular poly(3-alkylthiophene)s. *Nature Communications* **2011,** *2*, 1545-1-1545/8.
20. Pang, Y.; Li, J.; Hu, B.; Karasz, F. E. A Highly Luminescent Poly[(m-phenylenevinylene)-alt-(p-phenylenevinylene)] with defined conjugation length and improved solubility. *Macromolecules* **1999,** *32*, 3946-3950.
21. Yi, W.; Malkovskiy, A.; Chu, Q.; Sokolov, A. P.; Colon, M. L.; Meador, M.; Pang, Y. Wrapping of Single-Walled Carbon Nanotubes by a -Conjugated Polymer: The Role of Polymer Conformation-Controlled Size Selectivity. *J. Phys. Chem. B* **2008,** *112*, 12263-12269.

22. Chen, Y.; Xu, Y.; Perry, K.; Sokolov, A. P.; More, K.; Pang, Y. Achieving Diameter-Selective Separation of Single-Walled Carbon Nanotubes by Using Polymer Conformation-Confined Helical Cavity. *ACS Macro Letters* **2012,** 701-705.
23. Nelson, D. J.; Nagarajan, P. S.; Brammer, C. N.; Perumal, P. T. Effect of Single-Walled Carbon Nanotube Association upon 1H NMR Spectra of Representative Organonitrogen Compounds. *The Journal of Physical Chemistry C* **2010,** *114*, 10140-10147.
24. Weisman, R. B.; Bachilo, S. M. Dependence of Optical Transition Energies on Structure for Single-Walled Carbon Nanotubes in Aqueous Suspension: An Empirical Kataura Plot. *Nano Lett.* **2003,** *3*, 1235-1238.
25. Yi, W.; Malkovskiy, A.; Xu, Y.; Wang, X.; Sokolov, A. P.; Lebron-Colon, M.; Meador, M. A.; Pang, Y. Polymer conformation-assisted wrapping of single-walled carbon nanotube: The impact of cis-vinylene linkage. *Polymer* **2010,** *51*, 475-481.
26. The rotational barrier around a carbon-carbon triple bond is calculated to be ~0.64 kcal/mol. See S. Saebo, J. Almolof, J. E. Boggs, J. G. Stark. *J. Mol. Struct.* (THEOCHEM) **1989**, *200*, 361-373.
27. Chen, Y.; Xu, Y.; Wang, Q.; Gunasinghe, R. N.; Wang, X.-Q.; Pang, Y. Highly Selective Dispersion of Carbon Nanotubes by Using Poly(phenyleneethynylene)-Guided Supermolecular Assembly. Small **2013**, *9*, 870-875.
28. Tan, C.; Pinto, M. R.; Schanze, K. S. Photophysics, aggregation and amplified quenching of a water-soluble poly(phenylene ethynylene). *Chem. Comm.* **2002,** 446-447.
29. Pang, Y.; Li, J.; Hu, B.; Karasz, F. E. A Processible Poly(phenyleneethynylene) with Strong Photoluminescence: Synthesis and Characterization of Poly(m-phenyleneethynylene)-alt-(p-phenyleneethynylene)]. *Macromolecules* **1998,** *31*, 6730-6732.
30. Excitation (6,5) requires the use of laser frequency at about 575 nm, as seen from Figure 9b.
31. Ogunro, O. O.; Wang, X. Q. Quantum Electronic Stability in Selective Enrichment of Carbon Nanotubes. *Nano Lett.* **2009,** *9*, 1034-1038.
32. Lu, J.; Lai, L.; Luo, G.; Zhou, J.; Qin, R.; Wang, D.; Wang, L.; Mei, W. N.; Li, G.; Gao, Z.; Nagase, S.; Meada, Y.; Akasaka, T.; Yu, D. Why Semiconducting Single-Walled

Carbon Nanotubes are Separated from their Metallic Counterparts. *Small* **2007,** *3*, 1566-1576.

33. Chu, Q.; Pang, Y.; Ding, L.; Karasz, F. E. Green-Emitting PPE-PPV Hybrid Polymers: Efficient Energy Transfer across the *m*-Phenylene Bridge. *Macromolecules* **2003,** *36*, 3848-3853.
34. Yao, J.; Chen, Y.; Pang, Y. Application of Sonochemistry in the Isomerization of Carbon-Carbon double bond. *J. Polym. Sci. Part A: Polym. Chem.* **2010,** *48*, 5254-5257.
35. Yang, C. M.; Park, J. S.; An, K. H.; Lim, S. C.; Seo, K.; Kim, B.; Park, K. A.; Han, S.; Park, C. Y.; Lee, Y. H. Selective Removal of Metallic Single-Walled Carbon Nanotubes with Small Diameters by Using Nitric and Sulfuric Acids. *J. Phys. Chem. B* **2005,** *109*, 19242-19248.
36. Bahr, J. L.; Yang, J.; Kosynkin, D. V.; Bronikowski, M. J.; Smalley, R. E.; Tour, J. M. Functionalization of Carbon Nanotubes by Electrochemical Reduction of Aryl Diazonium Salts:ΓÇë A Bucky Paper Electrode. *J. Am Chem. Soc.* **2001,** *123*, 6536-6542.
37. Zhou, W.; Ooi, Y. H.; usso, R.; apanek, P.; Luzzi, D.; Fischer, J.; Bronikowski, M.; Willis, P.; Smalley, R. Structural characterization and diameter-dependent oxidative stability of single wall carbon nanotubes synthesized by the catalytic decomposition of CO. *Chemical Physics Letters* **2011,** *350*, 6-14.
38. Banerjee, S.; Wong, S. S. Demonstration of Diameter-Selective Reactivity in the Sidewall Ozonation of SWNTs by Resonance Raman Spectroscopy. *Nano Lett.* **2004,** *4*, 1445-1450.
39. The absorption peak of 1525 nm is close to the predicted V1-C1 transition(1516 nm) for (11,7).
40. Krupke, R.; Hennrich, F.; Lohneysen, H. V.; Kappes, M. M. Separation of Metallic from Semiconducting Single-Walled Carbon Nanotubes. *Science* **2003,** *301*, 344-347.
41. Arnold, M. S.; Green, A. A.; Hulvat, J. F.; Stupp, S. I.; Hersam, M. C. Sorting carbon nanotubes by electronic structure using density differentiation. *Nature Nanotechnol.* **2006,** *1*, 60-65.
42. Haroz, E. H.; Duque, J. G.; Lu, B. Y.; Nikolaev, P.; Arepalli, S.; Hauge, R. H.; Doorn, S. K.; Kono, J. Unique Origin of Colors of Armchair Carbon Nanotubes. *J. Am Chem. Soc.* **2012,** *134*, 4461-4464.

43. Moshammer, K.; Hennrich, F.; Kappes, M. M. Selective suspension in aqueous sodium dodecyl sulfate according to electronic structure type allows simple separation of metallic from semiconducting single-walled carbon nanotubes. *Nano Research* **2009,** *2* (8), 599-606.

44. Tu, X.; Hight Walker, A. R.; Khripin, C. Y.; Zheng, M. Evolution of DNA Sequences Toward Recognition of Metallic Armchair Carbon Nanotubes. *J. Am Chem. Soc.* **2011,** *133*, 12998-13001.

45. Maeda, Y.; Kimura, S.; Kanda, M.; Hirashima, Y.; Hasegawa, T.; Wakahara, T.; Lian, Y.; Nakahodo, T.; Tsuchiya, T.; Akasaka, T.; Lu, J.; Zhang, X.; Gao, Y.; Yu, Y.; Nagase, S.; Kazaoui, S.; Minami, N.; Shimizu, T.; Tokumoto, H.; Saito, R. Large-Scale Separation of Metallic and Semiconducting Single-Walled Carbon Nanotubes. *J. Am. CHem. Soc.* **2005,** *127*, 10287-10290.

46. Chattopadhyay, D.; Galeska, I.; Papadimitrakopoulos, F. A Route for Bulk Separation of Semiconducting from Metallic Single-Wall Carbon Nanotubes. *J. Am. CHem. Soc.* **2003,** *125*, 3370-3375.

47. Ju, S. Y.; Utz, M.; Papadimitrakopoulos, F. Enrichment Mechanism of Semiconducting Single-Walled Carbon Nanotubes by Surfactant Amines. *Journal of the American Chemical Society* **2009,** *131*, 6775-6784.

48. Mucalo, M.; Kato, K.; Yokogaw, Y. Phosphorylated, cellulose-based substrates as potential adsorbents for bone morphogenetic proteins in biomedical applications: A protein adsorption screening study using cytochrome *C* as a bone morphogenetic protein mimic. *Colloids and Surfaces B: Biointerfaces* **2009,** *71*, 52-58.

49. Doorn, S. K.; Araujo, P. T.; Hata, K.; Jorio, A. Excitons and exciton-phonon coupling in metallic single-walled carbon nanotubes: Resonance Raman spectroscopy. *Phys. Rev. B* **2008,** *78*, 165408/1-165408/9.

50. Haroz, E. H.; Rice, W. D.; Lu, B. Y.; Ghosh, S.; Hauge, R. H.; Weisman, R. B.; Doorn, S. K.; Kono, J. Enrichment of Armchair Carbon Nanotubes *via* Density Gradient Ultracentrifugation: Raman Spectroscopy Evidence. *ACS Nano* **2010,** *4*, 1955-1962.

51. Haroz, E. H.; Dugue, J. G.; Rice, W. D.; Densmore, C. G.; Kono, J.; Doom, S. K. Resonant Raman spectroscopy of armchair carbon nanotubes: Absence of broad *G*-feature. *Phys. Rev. B* **2011,** *84*, 121403.